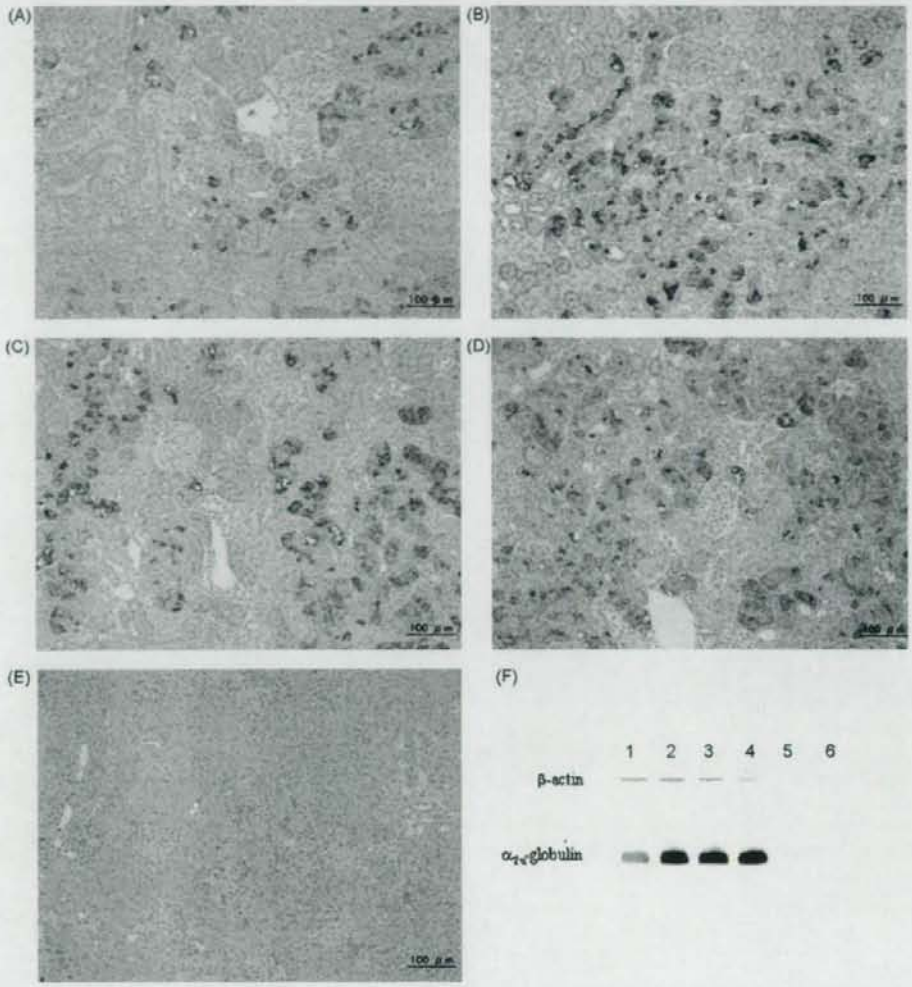

Fig. 3. Photomicrographs of immunohistochemical staining for α_{2u}-globulin in the kidneys of male (A–D) and female (E) *gpt* delta rats given DW (A), $KBrO_3$ (B), $KBrO_3$ and α-TP (C), $KBrO_3$ and SAA (D), or $KBrO_3$ (E). Western blot analysis of α_{2u}-globulin (F) from kidneys of male (lanes 1–4) and female (lanes 5 and 6) *gpt* delta rats given DW (lane 1), $KBrO_3$ (lane 2), $KBrO_3$ and α-TP (lane 3), $KBrO_3$ and SAA (lane 4), DW (lane 5), and $KBrO_3$ (lane 6). α_{2u}-globulin accumulation is more prominent in $KBrO_3$-treated male rats (B) as compared to the controls (A), and is not affected by α-TP (C) or SAA (D) treatment. Note the lack of accumulation in $KBrO_3$-treated females (E), in line with the Western blot analysis (F).

dose-dependent manner from 30 ppm, the protein levels being statistically significant at 125 ppm and above (Umemura et al., 2004). Therefore, it is very likely that this protein accumulation is involved in the cell proliferation observed in the males. In the present study, immunohistochemical and Western blot analysis of α_{2u}-globulin clearly demonstrated accumulation due to $KBrO_3$ exposure, which was not affected by either of antioxidants. This might account for the finding that simultaneous administration of SAA failed to block the rise in BrdU-LIs in males exposed to $KBrO_3$. In general, non-covalently binding of chemicals to the α_{2u}-globulin binding site, a highly aromatic region of the α_{2u}-globulin binding pocket (Huwe et al., 1996) seems to be an initial step, followed by accumulation of the protein in lysosomes of PCT because of resultant resistance to proteolysis. Alternatively, since activities of cystein proteases in lysosomes are prerequisite for degradation of α_{2u}-globulin (Saito et al., 1992), there might be the possibility of primary decrease of protease activity in lysosomes due to interaction of $KBrO_3$ with their thiols acting as a trigger for accumulation (Read, 1991). Although it remains uncertain whether $KBrO_3$ has affinity for the pocket or detrimental effects on lysomal functions, our data imply that induction of cell proliferation following accumulation of the protein in males occurs independently of oxidative stress. On the other hand, in the females lacking α_{2u}-globulin, the BrdU-LI elevation in PCT of rats given $KBrO_3$ was alleviated by SAA. Since mRNA levels of oxidative stress-related genes such as *c-fos*, *c-jun* and *NF-κB* were not elevated in kidneys of $KBrO_3$-treated female rats (data not shown), further studies appear warranted to determine links at the molecular level between oxidation and cell proliferation.

Exposure of female *gpt* delta rats with a genetic background of F344 to $KBrO_3$ at 500 ppm for 9 weeks induced significant elevation of *gpt* MFs along with Spi^- MFs. However, the antioxidants were unable to prevent any type of mutation. 8-OHdG is not only a

Table 2
Effects of antioxidants on *gpt* mutant frequencies in the kidneys of female *gpt* delta rats given $KBrO_3$.

Treatment		Animal no.	Cm^R colonies ($\times 10^5$)	6-TG^R and Cm^R colonies	Mutant frequency ($\times 10^{-5}$)	Mean ± SD
Water	Diet					
		51	9.9	3	0.30	
DW	BD	52	6.0	1	0.17	0.24 ± 0.07
		53	11.8	3	0.25	
		56	11.0	7	0.64	
$KBrO_3$	BD	57	9.6	4	0.42	0.53 ± 0.11*
		58	11.4	6	0.53	
		61	8.6	6	0.70	
$KBrO_3$	α-TP	62	9.5	4	0.42	0.48 ± 0.20
		63	13.0	4	0.31	
		66	6.8	2	0.29	
$KBrO_3$	SAA	67	10.2	2	0.20	0.44 ± 0.34
		68	8.4	7	0.83	

DW: Distilled water, BD: basal diet.
* $p < 0.01$ vs. DW/BD.

Table 3
Mutation spectra of *gpt* mutant colonies.

Sex	Male				Female			
Treatment (water/diet)	DW/BD	$KBrO_3$/BD	$KBrO_3$/α-TP	$KBrO_3$/SAA	DW/BD	$KBrO_3$/BD	$KBrO_3$/α-TP	$KBrO_3$/SAA
Base substitution								
Transversions								
GC:TA	0[a]	1(0.04)	4(0.17)	3(0.11)	2(0.07)	1(0.03)	0	2(0.08)
GC:CG	0	0	0	1(0.04)	0	1(0.03)	1(0.03)	1(0.04)
AT:TA	0	2(0.08)	4(0.17)	3(0.11)	0	3(0.09)	4(0.13)	2(0.08)
AT:CG	0	1(0.04)	2(0.08)	0	0	3(0.09)	0	0
Transitions								
GC:AT	2(0.09)	1(0.04)	8(0.34)	2(0.07)	2(0.07)	4(0.13)	6(0.19)	3(0.12)
AT:GC	0	1(0.04)	3(0.13)	1(0.04)	0	1(0.03)	1(0.03)	0
Deletion								
Single bp	0	1(0.04)	3(0.13)	1(0.04)	2(0.07)	6(0.19)	2(0.06)	1(0.04)
Over 2 bp	0	1(0.04)	2(0.08)	2(0.07)	1(0.04)	1(0.03)	0	1(0.04)
Insertion	0	1(0.04)	0	0	0	0	1(0.03)	1(0.04)
Complex	1(0.04)	1(0.04)	0	0	0	0	1(0.03)	0
Total	3(0.13)	10(0.39)	26(1.09)	14(0.51)	7(0.25)	20(0.63)*	14(0.51)	11(0.63)

DW: Distilled water, BD: basal diet. Values appearing in parenthesis indicates mutation frequency, $\times 10^{-5}$. * $p < 0.01$ vs. DW/BD.
[a] The number of colonies with independent mutations.

representative marker for oxidative stress but also a primary cause of GC:TA transversions due to mispairing with A (Cheng et al., 1992; Shibutani et al., 1991). Nevertheless, spectrum analysis of the *gpt* mutants induced by $KBrO_3$ did not indicate a majority of GC:TA transversions. Instead, deletions were most common in concord with the results of Spi^- mutation assays. In our previous study using male *gpt* delta rats with a Sprague–Dawley genetic background, significant elevation of Spi^- MFs was rather apparent (Umemura et al., 2006). Furthermore, in an *in vitro* genotoxicity assay for $KBrO_3$ using human lymphoblastoid TK6 cells (Luan et al., 2007) or mouse lymphoma cells (Harrington-Brock et al., 2003), $KBrO_3$ induced large deletions, including loss of heterozygosity at

Table 4
Effects of antioxidants on *red/gam* mutant frequencies in the kidneys of male *gpt* delta rats given $KBrO_3$.

Treatment		Animal no.	Plaques within XL-1 Blue MRA ($\times 10^5$)	Plaques within XL-1 Blue MRA (P2) (Spi^-)	Mutant frequency ($\times 10^{-5}$)	Mean ± SD
Water	Diet					
		1	19.2	8	0.42	
DW	BD	2	20.3	13	0.64	0.82 ± 0.52
		3	17.8	25	1.40	
		6	15.3	36	2.36	
$KBrO_3$	BD	7	21.8	8	0.37	1.04 ± 1.15
		8	15.7	6	0.38	
		11	23.4	9	0.39	
$KBrO_3$	α-TP	12	26.0	11	0.42	0.43 ± 0.05
		13	14.3	7	0.49	
		16	17.8	9	0.51	
$KBrO_3$	SAA	17	14.5	8	0.55	0.57 ± 0.08
		18	19.5	13	0.67	

DW: Distilled water, BD: basal diet.

Table 5
Effects of antioxidants on *red/gam* mutant frequencies in the kidneys of female *gpt* delta rats given $KBrO_3$.

Treatment		Animal no.	Plaques within XL-1 Blue MRA ($\times 10^5$)	Plaques within XL-1 Blue MRA (P2) (Spi^-)	Mutant frequency ($\times 10^{-5}$)	Mean ± SD
Water	Diet					
DW	BD	51	15.2	2	0.13	0.45 ± 0.30
		52	6.8	5	0.73	
		53	10.5	5	0.48	
$KBOrO_3$	BD	56	5.2	6	1.16	0.89 ± 0.42
		57	4.9	2	0.41	
		58	6.4	7	1.09	
$KBrO_3$	α-TP	61	5.6	7	1.24	1.02 ± 0.20*
		62	8.4	8	0.96	
		63	3.5	3	0.85	
$KBrO_3$	SAA	66	5.2	8	1.55	0.97 ± 0.51
		67	7.0	5	0.71	
		68	7.8	5	0.64	

DW: Distilled water, BD: basal diet.
* $p < 0.05$ vs. DW/BD.

TK locus, but not GC:TA transversions. On the other hand, in the present study, Spi^- MFs in males were not increased, in contrast to the previous study demonstrating significant increment. Although certain differences between genetic backgrounds should not be ignored, seemingly inconsistent results might reflect smaller increase of MFs following $KBrO_3$ exposure (2–3 fold) as compared to the case (10–30 fold) with potent genotoxic carcinogens (Kanki et al., 2005). In other words, as shown in microbial and the *Hprt* mutation assays in mammalian cells (Speit et al., 1999), the potential of $KBrO_3$ to induce mutations may be very weak (Harrington-Brock et al., 2003). Actually, we obtained negative data for transgene mutations at 250 ppm for 13 weeks (Umemura et al., 2006) and another group similarly reported negative findings with 125 ppm for 16 weeks (Yamaguchi et al., 2008). The hypothesis of weak mutagenicity is strongly supported by a bioassay showing $KBrO_3$ at 500 ppm for 13 weeks to be incapable of effecting tumor development with appropriate promotion, despite preneoplastic lesions being enhanced (Umemura et al., 2006).

In conclusion, oxidative stress generated by $KBrO_3$ might take part in induction of cell proliferation in PCT of female rats, leading to tumor promoting potential. In males, in contrast, α_{2u}-globulin accumulation independent of oxidative stress plays a major role in cell proliferation, which implies that the tumor promotion observed in males is not directly comparable to the human situation. Likewise, induction of reporter gene mutations by $KBrO_3$ is unlikely to be due to oxidative stress, the extent of which being much lower as compared to that of potent genotoxic carcinogens. The data overall allow us to speculate that the predominant contributing factor for $KBrO_3$-induced renal carcinogenesis is tumor promoting potential, which is only to a limited extent associated with oxidative stress.

Conflict of interest

None.

Acknowledgements

We thank Ms. Ayako Kaneko and Yoshimi Komatsu for expert technical assistance in processing histological materials. This work was supported in part by a Grant-in-Aid for Cancer Research from the Ministry of Health, Labor and Welfare, Japan.

References

Ballmaier, D., Epe, B., 1995. Oxidative DNA damage induced by potassium bromate under cell-free condition and in mammalian cells. Carcinogenesis 16, 335–342.
Ballmaier, D., Epe, B., 2006. DAN damage by bromate: mechanism and consequence. Toxicologoy 221, 166–171.
Cadenas, S., Barja, G., 1999. Resveratrol, melatonin, vitamin E, and PBN protect against renal oxidative DNA damage induced by the kidney carcinogen $KBrO_3$. Free Radic. Biol. Med. 26, 1531–1537.
Cavanagh, J.E., Weinberg, H.S., Gold, A., Sangalah, R., Marbury, D., Glase, W.H., Collette, T.W., Richardson, S.D., Thruston, A.D., 1992. Ozonation of byproducts: identification of bromohydrins from the ozonation of natural waters with enhanced bromide levels. Environ. Sci. Technol. 26, 1658–1662.
Cheng, K.C., Cahill, D.S., Kasai, H., Nishimura, S., Loeb, L.A., 1992. 8-hydroxyguanine, an abundant form of oxidative DNA damage, causes G:T and A:C substitutions. J. Biol. Chem. 267, 166–172.
Chipman, J.K., Davies, J.E., Parsons, J.L., Nair, J., O'Neill, G., Fawell, J.K., 1998. DNA oxidation by potassium bromate; a direct mechanism or linked to lipid peroxidation? Toxicology 126, 93–102.
Craven, P.A., Derubertis, F.R., Kagan, V.E., Melhem, M., Studer, R.K., 1997. Effects of supplementation with vitamin C or E on albuminuria, glomerular TGF-β, and glomerular size in diabetes. J. Am. Soc. Nephrol. 8, 1405–1414.
DeAngelo, A., George, M.H., Kilburn, S.R., Moore, T.M., Wolf, D.C., 1998. Carcinogenicity of potassium bromate administered in the drinking water to B6C3F1 mice and F344/N rats. Toxicol. Pathol. 26, 587–594.
Delker, D., Hatch, G., Allen, J., Crissman, B., George, M., Geter, D., Kilburn, S., Moore, T., Nelson, G., Roop, B., et al., 2006. Molecular biomarkers of oxidative stress associated with bromate carcinogenicity. Toxicology 221, 158–165.
El-Sokkary, G.H., 2000. Melatonin protects against oxidative stress induced by the kidney carcinogen $KBrO_3$. Neroendocrinol. Lett. 21, 461–468.
Harrington-Brock, K., Collard, D.D., Chen, T., 2003. Bromate induces loss of heterozygosity in the *Thymidine kinase gene* of L5178Y/$Tk^{+/-}$-3.7.2C mouse lymphoma cells. Mutat. Res. 537, 21–28.
Hayashi, M., Kishi, M., Sofuni, T., Ishidate, M., 1988. Micronucleus tests with mice on 39 food additives and 8 miscellaneous chemical substances. Food Chem. Toxicol. 26, 487–500.
Helbock, H.J., Beckman, K.B., Shigenaga, M.K., Walter, P.B., Woodall, A.A., Yeo, H.C., Ames, B.N., 1998. DNA oxidation matters: the HPLC-electrochemical detection assay of 8-oxo-deoxyguanosine and 8-oxo-deoxyguanine. Proc. Natl. Acad. Sci. U.S.A. 95, 288–293.
Huwe, J.K., Larsen, G.L., Castellino, S., 1996. An investigation of the binding site of α_{2u}-globulin using isotopically labeled ligands and inverse nuclear magnetic resonance techniques. Chem. Res. Toxicol. 9, 215–222.
Ishidate, M., Yoshioka, K., 1980. Chromosome aberration tests with Chinese hamster cells in vitro with and without metabolic activation: a comparative study on mutagens and carcinogens. Arch. Toxicol. (Suppl. 4), 41–44.
Ishidate, M., Sofuni, T., Yoshikawa, K., Hayashi, M., Nohmi, T., Sawada, T., Matsuoka, A., 1984. Primary mutagenicity screening of food additives currently used in Japan. Food Chem. Toxicol. 22, 623–636.
Kaya, F.F., Topaktas, M., 2007. Genotoxic effects of potassium bromate on human peripheral lymphocytes *in vitro*. Mutat. Res. 626, 48–52.
Kasai, H., Nishimura, S., 1991. Formation of 8-hydroxydeoxyguanosine in DNA by oxygen radicals and its biological significance. In: Sies, H. (Ed.), Oxidative Stress: Oxidant and Antioxidants. Academic Press, London, pp. 99–116.
Kasai, H., 2002. Chemistry-based studies on oxidative DNA damage: formation, repair, and mutagenesis. Free Radic. Biol. Med. 33, 450–456.
Kanki, K., Nishikawa, A., Masumura, K., Umemura, T., Imazawa, T., Kitamura, Y., Nohmi, T., Hirose, M., 2005. *In vivo* mutational analysis of liver DNA in *gpt* delta transgenic rats treated with the hepatocarcinogens *N*-nitrosopyrrolidine, 2-amino-3-methylimidazo[4,5-*f*]quinoline, and de(2-ethylhexyl)phthalate. Mol. Carcinog. 42, 9–17.
Kurokawa, Y., Aoki, S., Imazawa, T., Hayashi, Y., Matsushima, Y., Takamura, N., 1985. Dose-related enhancing effect of potassium bromate on renal tumorigenesis in rats initiated with *N*-ethyl-*N*-hydroxyethyl-nitrosamine. Jpn. J. Cancer Res. 76, 583–589.

Kurokawa, Y., Takayama, S., Konishi, Y., Hiasa, Y., Asahina, S., Takahashi, M., Maekawa, A., Hayashi, Y., 1986. Long-term *in vivo* carcinogenicity tests of potassium bromate, sodium hypochlorite, and sodium chlorite conducted in Japan. Environ. Hlth. Perspect. 69, 221–235.

Kurokawa, Y., Maekawa, A., Takahashi, M., Hayashi, Y., 1990. Toxicity and carcinogenicity of potassium bromate—a new renal carcinogen. Environ. Hlth. Perspect. 87, 309–335.

Luan, Y., Suzuki, T., Palanisamy, R., Takashima, Y., Sakamoto, H., Sakuraba, M., Koizumi, T., Saito, M., Matsufuji, H., Yamagata, K., 2007. Potassium bromate treatment predominantly causes large deletions, but not GC > TA transversion in human cells. Mutat. Res. 619, 113–123.

Murata, M., Bansho, Y., Inoue, S., Ito, K., Ohnishi, S., Midorikawa, K., Kawanishi, S., 2001. Requirement of glutathione and cysteine in guanine-specific oxidation of DNA by carcinogenic potassium bromate. Chem. Res. Toxicol. 14, 678–685.

Nakae, D., Mizumoto, Y., Kobayashi, E., Noguchi, O., Konishi, Y., 1995. Improved genomic/nuclear DNA extraction for 8-hydroxydeoxyguanosine analysis of small amounts of rat liver tissue. Cancer Lett. 97, 233–239.

Nesslany, F., Zennouche, N., Simar-Neintieres, S., Talahari, I., NKili-Mboui, E.-N., Marzin, D., 2007. In vivo comet assay on isolated kidney cells to distinguish genotoxic carcinogens from epigenetic carcinogens or cytotoxic compounds. Mutat. Res. 630, 28–41.

Nohmi, T., Suzuki, T., Masumura, K., 2000. Recent advances in the protocols of transgenic mouse mutation assays. Mutat. Res. 455, 191–215.

Read, N.G., 1991. The role of lysomes in hyaline droplet nephropathy induced by a variety of pharmacological agents in the male rat. Histochem. J. 23, 436–443.

Rutenburg, A.M., Kim, H., Fiscbein, J.W., Hanker, J.S., Wasserkrug, H.L., Seligman, A.M., 1969. Histochemical and ultrastructural demonstration of gamma-transpepdidase activity. J. Histochem. Cytochem. 1, 517–526.

Sai, K., Hayashi, M., Takagi, A., Hasegawa, R., Sofuni, T., Kurokawa, Y., 1992. Effects of antioxidants on induction of micronuclei in rat peripheral blood reticulocytes by potassium bromate. Mutat. Res. 269, 113–118.

Saito, K., Kaneko, H., Isobe, N., Nakatsuka, I., Yoshitake, A., Yamada, H., 1992. Differences in α_{2u}-globulins increased in male rat kidneys following treatment with several α_{2u}-globulin accumulating agents: cystein protease(s) play(s) an important role in production of kidney-type-α_{2u}-globulin. Toxicology 76, 177–186.

Shibutani, S., Takeshita, M., Grollman, A.P., 1991. Insertion of specific bases during DNA synthesis past the oxidation damaged base 8-oxodG. Nature 191, 431–434.

Speit, G., Haupter, S., Schutz, P., Kreis, P., 1999. Comparative evaluation of the genotoxic properties of potassium bromate and potassium superoxide in V79 Chinese hamster cells. Mutat. Res. 439, 213–221.

Umemura, T., Tokumo, K., Williams, G.M., 1992. Cell proliferation induced in the kidneys and livers of rats and mice by short term exposure to the carcinogen p-dichlorobenzene. Arch. Toxicol. 66, 503–507.

Umemura, T., Sai, K., Takagi, A., Hasegawa, R., Kurokawa, Y., 1993. A possible role for cell proliferation in potassium bromate ($KBrO_3$) carcinogenesis. J. Cancer Res. Clin. Oncol. 119, 463–469.

Umemura, T., Sai, K., Takagi, A., Hasegawa, R., Kurokawa, Y., 1995. A possible role for oxidative stress in potassium bromate ($KBrO_3$). Carcinogenesis 16, 593–597.

Umemura, T., Takagi, A., Sai, K., Hasegawa, R., Kurokawa, Y., 1998. Oxidative DNA damage and cell proliferation in kidneys of male and female rats during 13-week exposure to potassium bromate ($KBrO_3$). Arch. Toxicol. 72, 264–269.

Umemura, T., Kimura, Y., Kanki, K., Maruyama, S., Okazaki, K., Imazawa, T., Nishimura, T., Hasegawa, R., Nishikawa, A., Hirose, M., 2004. Dose-related changes of oxidative stress and cell proliferation in kidneys of male and female F344 rats exposed to potassium bromate. Cancer Sci. 95, 393–398.

Umemura, T., Kurokawa, Y., 2006. Etiology of bromate-induced cancer and possible modes of action-studies in Japan. Toxicology 221, 154–157.

Umemura, T., Kanki, K., Kuroiwa, Y., Ishii, Y., Okano, K., Nohmi, T., Nishikawa, A., Hirose, M., 2006. In vivo mutagenicity and initiation following oxidative DNA lesion in the kidneys of rats given potassium bromate. Cancer Sci. 97, 829–835.

Umemura, T., Kuroiwa, Y., Tasaki, M., Okamura, T., Ishii, Y., Kodama, Y., Nohmi, T., Mitsumori, K., Nishikawa, A., Hirose, M., 2007. Detection of oxidative DNA damage, cell proliferation and in vivo mutagenicity induced by dicyclanil, a non-genotoxic carcinogen, using *gpt* delta mice. Mutat. Res. 633, 46–54.

Yamaguchi, T., Wei, M., Hagihara, N., Omori, M., Wanibuchi, H., Fukushima, S., 2008. Lack of mutagenic and toxic effects of low dose potassium bromate on kidneys in the Big Blue rat. Mutat. Res. 652, 1–11.

Crosstalk between PTEN/Akt2 and TGFβ signaling involving EGF receptor down-regulation during the tumor promotion process from the early stage in a rat two-stage hepatocarcinogenesis model

Eriko Taniai,[1] Masaomi Kawai,[1,2] Yasuaki Dewa,[1,2] Jihei Nishimura,[1,2] Tomoaki Harada,[1] Yukie Saegusa,[1,2] Sayaka Matsumoto,[1,2] Miwa Takahashi,[3] Kunitoshi Mitsumori[1] and Makoto Shibutani[1,4]

[1]Laboratory of Veterinary Pathology, Tokyo University of Agriculture and Technology, Tokyo; [2]Pathogenetic Veterinary Science, United Graduate School of Veterinary Sciences, Gifu; [3]Division of Pathology, National Institute of Health Sciences, Tokyo, Japan

(Received November 11, 2008/Revised January 7, 2009; January 17, 2009/Accepted January 21, 2009)

The present study investigated the involvement of signaling of phosphatase and tensin homolog deleted on chromosome 10 (PTEN)/protein kinase B (Akt) and transforming growth factor-β (TGFβ) as well as receptor tyrosine kinases in the tumor promotion processes in a two-stage hepatocarcinogenesis model using male F344 rats. The cellular localization of related molecules was examined in liver cell foci expressing glutathione *S*-transferase placental form (GST-P) at the early stage of tumor promotion by fenbendazole (FB), piperonyl butoxide, or thioacetamide. Distribution in the liver cell foci and neoplastic lesions positive for GST-P was also examined at the later stage of FB promotion. In contrast to the initiation-alone cases, subpopulations of GST-P-positive foci induced by promotion for 6 weeks, regardless of the promoting chemicals used, enhanced down-regulation of PTEN and up-regulation of phosphorylated (active) Akt2 and phosphorylated substrate(s) of Akt-kinase activity. Also, up-regulation of TGFβ receptor I and down-regulation of epidermal growth factor receptor (EGFR) were enhanced in the subpopulation of GST-P-positive foci in all promoted cases. A similar pattern of cellular distribution of these molecules was also observed in the neoplastic lesions at the late stage. These results suggest a crosstalk between Akt2 and TGFβ signaling that involves a mechanism requiring EGFR down-regulation during the entire tumor promotion process starting from the early stage. In particular, a shift in subcellular localization of phosphorylated substrate(s) of Akt from the cell membrane in liver cell foci to the cytoplasm in carcinomas was observed, suggesting an alteration of the function or activity of the corresponding molecule(s). (*Cancer Sci* 2009)

In a rat two-stage hepatocarcinogenesis model, altered liver cell foci immunoreactive for glutathiuone *S*-transferase placental form (GST-P) have been shown to increase in number and area because of tumor promotion with hepatocarcinogens, in accordance with the hepatocarcinogenic potential; therefore, these foci have been confirmed as preneoplastic lesions of liver cells.[1,2] However, only a few studies have examined the roles of cellular signaling and molecular linkage in the growth and development of the liver cell foci.[3–6]

Akt is a serine/threonine kinase that is a central regulator of widely divergent cellular processes, including proliferation, differentiation, migration, survival, and metabolism.[7] Akt is activated by a variety of stimuli, through growth factor receptors, in a phosphatidylinositol 3-kinase (PI3K)-dependent manner, and it is also negatively regulated by the tumor suppressor phosphatase and tensin homolog deleted on chromosome 10 (PTEN).[8] A disruption of normal Akt/PTEN signaling frequently occurs in many human cancers, and thus these molecules play an important role in cancer development, progression, and therapeutic resistance.[9,10] To date, three members of the Akt family have been identified in mammals: Akt1, Akt2, and Akt3.[11] All three are ubiquitously expressed in all cell types and tissues, although Akt3 has a more restricted expression pattern. In rat hepatocarcinogenesis, there is a subpopulation of GST-P-positive liver cell foci exhibiting increased expression of PTEN and decreased expression of the phosphorylated (activated) form of Akt (phospho-Akt), as well as high levels of ceramide species that are sensitive to sphingomyelin as a chemopreventive target.[12] On the other hand, in a two-stage hepatocarcinogenesis model, we recently obtained a contradictory result showing a lack of PTEN expression in a majority of GST-P-positive foci induced by promotion with phenob-arbito (PB) or fenben-dazole (FB), in contrast to the constitutive expression of PTEN in surrounding hepatocytes.[13] This result suggests a decrease in the tumor suppressor function of PTEN by down-regulation even during the early stage of hepatocarcinogenesis.

In the above-mentioned study, we also found that transforming growth factor-β receptor I (TGFβRI) was coexpressed with GST-P in liver cell foci induced by promotion with PB or FB.[13] Growth factor signaling through the activation of receptor tyrosine kinase (RTK) is crucial for regulation of PI3K/Akt signaling.[14] Interestingly, TGFβ is able to activate PI3K/Akt in fetal hepatocytes by a mechanism dependent on activities of the erbB family RTK, epidermal growth factor receptor (EGFR), and c-Src.[15]

Here, to clarify the involvement of Akt/PTEN signaling during the early stage of hepatocarcinogenesis, we further examined the cellular distribution of molecules related to PTEN/Akt signaling in preneoplastic lesions induced by 6 weeks of tumor promotion. For this purpose, three non-genotoxic hepatocarcinogens, i.e. FB, piperonyl butoxide (PBO), and thioacetamide (TAA), were used as tumor-promoting chemicals. We also examined immunolocalization of TGFβRI, as well as RTKs such as erbB family proteins, in these preneoplastic lesions. Moreover, immunolocalization of representative molecules were further examined in proliferative lesions developed after 57 weeks of promotion with FB to pursue involvement during the later stage of tumor promotion.

[4]To whom correspondence should be addressed. E-mail: mshibuta@cc.tuat.ac.jp

Abbreviations: Ab, antibody; Akt, protein kinase B; Bcl2, B-cell CLL/lymphoma 2; c-erbB2, v-erb-b2 erythroblastic leukemia viral oncogene homolog 2; DEN, *N*-diethylnitrosamine; EGFR, epidermal growth factor receptor; FB, fenbendazole; Grb10, growth factor receptor bound protein 10; GST-P, glutathione *S*-transferase placental form; IGF-IRβ, insulin-like growth factor-I receptor β; *Mdm2*, transformed mouse 3T3 cell double minute 2; PB, phenobarbital; PBO, piperonyl butoxide; phospho-Akt, phosphorylated (activated) form of Akt; phospho-Akt2, phosphorylated (active) Akt2; phospho-PTEN, phosphorylated form of PTEN; PI3K, phosphatidylinositol 3-kinase; PTEN, phosphatase and tensin homolog deleted on chromosome 10; Raf-1, v-raf-leukemia viral oncogene 1; RTK, receptor tyrosine kinase; SDS-PAGE, sodium dodecyl sulfate–polyacrylamide gel electrophoresis; TAA, thioacetamide; TGF, transforming growth factor; TGFβRI, transforming growth factor-β receptor I.

doi: 10.1111/j.1349-7006.2009.01120.x

Materials and Methods

Chemicals. FB (CAS no. 43210-67-9) and *N*-diethylnitrosamine (DEN) (CAS no. 55-18-5) were purchased from Sigma-Aldrich Japan (Tokyo, Japan). PBO (CAS no. 51-03-6) was obtained from Nagase & Co. (Osaka, Japan), and TAA (CAS no. 62-55-5) was obtained from Wako Pure Chemicals Industries (Osaka, Japan).

Animal experiments. For analysis during the early stage of tumor promotion, 30 5-week-old male F344/NS1c rats were purchased from Japan SLC (Hamamatsu, Japan) and acclimatized on powdered basal diet (Oriental Yeast Co., Tokyo, Japan) and tap water ad libitum for 1 week. They were housed in stainless-steel cages in a barrier-maintained animal room on a 12-h light–dark cycle and conditioned at 23 ± 2°C with a relative humidity of 55 ± 15%.

At 6 weeks of age, animals were subjected to two-stage hepatocarcinogenesis using a medium-term liver bioassay.[1,2] All animals were initiated with a single intraperitoneal injection of DEN (200 mg/kg, dissolved in saline). Two weeks later, animals were divided into four groups and were fed basal diet (DEN-alone) or diet containing either FB at 3600 p.p.m. (DEN + FB), PBO at 20 000 p.p.m. (DEN + PBO), or TAA at 400 p.p.m. (DEN + TAA). The animals were subjected to two-thirds partial hepatectomy at week 3. At week 8, the animals were killed under deep ether anesthesia by exsanguinations from the abdominal aorta, and their livers were immediately removed and weighed. The liver slices were fixed in phosphate-buffered 4% paraformaldehyde solution (pH 7.4) for 2 days and processed for histopathological examinations. Small portions of liver tissues, approximately 100 mg, were excised, quickly frozen in liquid nitrogen, and stored at –80°C. The selected doses of FB, PBO, and TAA have been reported to show tumor-promoting activity or carcinogenic activity.[16–18]

To investigate the cellular distribution of molecules in neoplastic lesions during the late stage of tumor promotion, 35 F344/DuCrj rats (Charles River Japan, Yokohama, Japan) were promoted with FB at 3600 p.p.m. in the diet for 57 weeks.[13] The livers of surviving animals were removed, and the liver slices containing gross neoplastic lesions were processed for histopathological examination as described previously.

The animal protocols were reviewed and approved by the Animal Care and Use Committee of the Tokyo University of Agriculture and Technology (short-term study of 6-week promotion) and the National Institute of Health Sciences, Japan (long-term study of 57-week promotion).

Immunohistochemistry. Paraffin-embedded liver sections were subjected to immunohistochemistry using the horseradish peroxidase avidin–biotin complex method utilizing a VECTASTAIN Elite ABC Kit (Vector Laboratories, Burlingame, CA, USA) with 3,3′-diaminobenzidine/H_2O_2 as the chromogen. Rabbit polyclonal Ab against GST-P (1:1000; MBL, Nagoya, Japan) was used for all cases obtained at both 6 and 57 weeks of tumor promotion. In the livers after 6 weeks of promotion, serial sections were subjected to immunohistochemistry for EGFR (mouse monoclonal Ab, clone 6F1, 1:10; MBL), c-erbB2 (mouse monoclonal Ab, clone SPM495, 1:50; Thermo Fisher Scientific, Fremont, CA, USA), TGFβRI (rabbit polyclonal Ab, 1:50; Santa Cruz Biotechnology, Santa Cruz, CA, USA), insulin-like growth factor-I receptor β (IGF-IRβ) (rabbit polyclonal Ab, 1:150; Cell Signaling Technology, Danvers, MA, USA), PTEN (rabbit monoclonal Ab, clone 138G6, 1:100; Cell Signaling Technology), phosphorylated form of PTEN (phospho-PTEN; rabbit polyclonal Ab, 1:100; Cell Signaling Technology), Akt1 (mouse monoclonal Ab, clone 2H10, 1:50, Cell Signaling Technology), Akt2 (rabbit monoclonal Ab, clone 54G8, 1:150, Cell Signaling Technology), Akt3 (rabbit polyclonal Ab, 1:25, Cell Signaling Technology), phospho-Akt at the position of Ser473 (rabbit monoclonal Ab, clone 193H12, 1:50; Cell Signaling Technology), phospho-Akt2 (rabbit polyclonal Ab, 1:100; Abcam, Cambridge, UK), phospho-(Ser/Thr) Akt substrate detecting phosphorylated Akt substrate peptides (rabbit polyclonal Ab, 1:250; Cell Signaling Technology), 14-3-3 (rabbit polyclonal Ab, 1:40; Abcam), growth factor receptor bound protein 10 (Grb10) (rabbit polyclonal Ab, A-18, 1:20; Santa Cruz Biotechnology), Raf-1 (rabbit polyclonal Ab, 1:50; Abcam) or Synip (rabbit monoclonal Ab, clone EP302Y, 1:250; Epitomics, Burlingame, CA, USA). Phospho-PTEN is an inactive form of PTEN, and phospho-Akt and phospho-Akt2 are the active forms of Akt and Akt2, respectively. Because of the immunoreactivity of phospho-Akt substrate(s) on the cell surface of GST-P-positive liver cell foci, 14-3-3, Grb10, Raf-1, and Synip were selected as candidate substrates for Akt-kinase activity that can localize to cellular membrane.[19–25]

For cases after 57 weeks of tumor promotion with FB, 10 slices that included tumor nodules were selected (one slice/animal), and serial sections were subjected to immunohistochemistry for Akt1, Akt2, Akt3, phospho-Akt, phospho-Akt2, phospho-Akt substrate, 14-3-3, Grb10, TGFβRI, EGFR, c-erbB2, and IGF-IRβ.

For antigen retrieval, the sections were heated to 120°C in 10 mM citrate buffer (pH 6.0) by autoclaving for 10 min before incubation with each antibody.

Analysis of immunolocalization. The number and areas of GST-P-positive foci larger than 0.2 mm in diameter and the total areas of liver sections at week 6 of tumor promotion were measured using the WinROOF image analysis software package (version 5.7; Mitani Corp., Fukui, Japan), and then the number and areas of foci per unit area (cm^2) of liver section were calculated. For evaluation of the expression of EGFR, TGFβRI, PTEN, phospho-PTEN, phospho-Akt2, 14-3-3, and Grb10, immunoreactivity was classified as increased, unchanged, or decreased in the GST-P-positive foci as compared with the expression levels of surrounding liver cells. For this evaluation, up to 50 GST-P-positive foci were randomly selected per animal. For the study of proliferative lesions generated after promotion with FB for 57 weeks, liver cell foci, adenomas and carcinomas in 10 animals showing immunoreactivity with GST-P were examined by evaluation of immunoreactivity similarly to that of GST-P-positive foci at week 6 of promotion.

Expression analysis of polypeptide signals. Western blotting was performed with liver tissues at 6 weeks of tumor promotion ($N = 2$/group). With the same antibody used for immunohistochemistry, polypeptide signal levels of GST-P, phospho-Akt2, phospho-Akt substrate, or TGFβRI were examined utilizing chemiluminescent reaction with ECL Plus Western Blotting Detection Reagents (GE Healthcare UK, Little Chalfont, UK). Tissue extraction and estimation of protein concentration were performed according to the methods described previously,[26] and 10 μg of tissue extract was applied to 10% sodium dodecyl sulfate–polyacrylamide gel electrophoresis (SDS-PAGE). Resolved polypeptides were then transferred to a polyvinylidine difluoride membrane (Millipore, Billerica, MA, USA). Dilutions of applied Ab were 1:1000 for GST-P, phospho-Akt2, and phospho-Akt substrate, and 1:200 for TGFβRI. Goat antirabbit IgG-HRP (1:5000; Santa Cruz Biotechnology) was used as a secondary antibody. After signal detection of each molecule, membranes were reprobed with actin (1:200; Sigma, St. Louis, MO, USA) as a control for sample loading. Because GST-P is known to be expressed, cell lysate from a rat hepatoma cell line, H-4-II-E, was also included in the expression analysis.[27] Signal level was estimated by measuring band intensity with the WinROOF image analysis software package.

Statistical analysis. Variance in data for the numbers and areas of GST-P-positive foci were checked for homogeneity using Bartlett's procedure. If the variance was homogenous, the data were assessed by one-way ANOVA. If not, the Kruskal–Wallis test was applied. When statistically significant differences were indicated, Dunnett's multiple comparison test was employed for comparison with the DEN-alone group. Concordance ratios of the immunoreactive or immunonegative foci for molecules of interest with GST-P-positive foci were analyzed by χ^2-test for comparison between the DEN-alone group and each treatment group.

doi: 10.1111/j.1349-7006.2009.01120.x

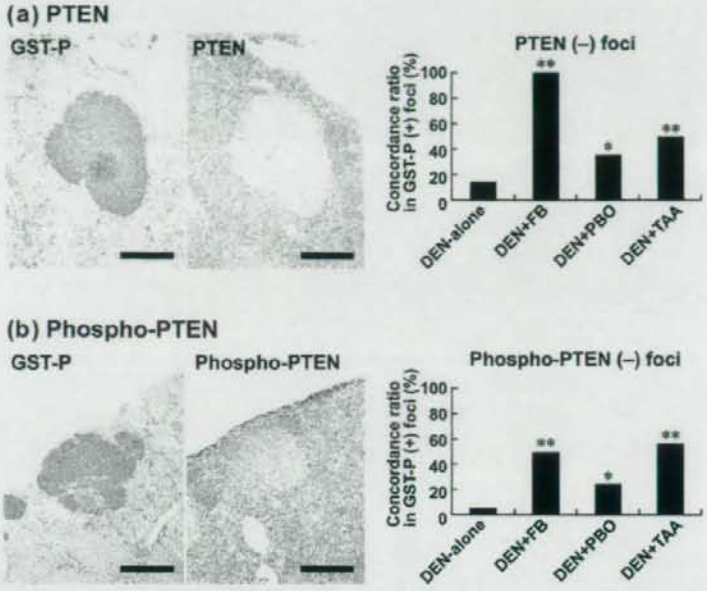

Fig. 1. Immunohistochemical localization of phosphatase and tensin homolog deleted on chromosome 10 (PTEN) and phospho-PTEN in association with glutathione *S*-transferase placental form (GST-P)-positive liver cell foci after promotion for 6 weeks. (a) Lack of PTEN expression (right) in a GST-P-positive focus (left) in the liver of a rat promoted with 3600 p.p.m. fenbendazole (FB) after *N*-diethylnitrosamine (DEN) initiation. Bar = 500 μm. The graph shows concordance ratios (%) of PTEN negativity with GST-P-positive foci generated after promotion with FB, piperonyl butoxide (PBO), or thioacetamide (TAA). *, **: $P < 0.05$, 0.01 *versus* DEN-alone group (χ^2-test). (b) Lack of phospho-PTEN expression (right) in a GST-P-positive focus (left) in the liver of a rat promoted with 3600 p.p.m. FB after DEN initiation. Bar = 500 μm. The graph shows concordance ratios (%) of phospho-PTEN negativity with GST-P-positive foci generated after promotion with FB, PBO, or TAA. *, **: $P < 0.05$, 0.01 *versus* DEN-alone group (χ^2-test).

Table 1. Quantitative data for GST-P-positive liver cell foci after promotion with FB, PBO, or TAA for 6 weeks

Group	No. of animals examined	GST-P-positive foci	
		Number (No./cm²)	Area (mm²/cm²)
DEN-alone	4	3.17 ± 1.05†	0.38 ± 0.14
DEN + FB 3600 p.p.m.	8	28.35 ± 9.43*	8.41 ± 4.46*
DEN + PBO 20 000 p.p.m.	9	13.60 ± 7.11	2.30 ± 1.83
DEN + TAA 400 p.p.m.	9	58.34 ± 9.57**	22.96 ± 5.39**

†Mean ± SD.
*, **: $P < 0.05$, $P < 0.01$ *versus* DEN-alone (Dunnett's test or Dunnett-type rank-sum test).
DEN, *N*-diethylnitrosamine; FB, fenbendazole; GST-P, glutathione *S*-transferase placental form; PBO, piperonyl butoxide; TAA, thioacetamide.

Results

Immunolocalization during the early stage of tumor promotion. At week 6 of tumor promotion with FB or TAA, both the number and area of GST-P-positive liver cell foci were significantly increased compared with those in the DEN-alone group (Table 1). Although statistically non-significant, the number and area of GST-P-positive foci were also increased by promotion with PBO.

Liver cells without GST-P-positive foci were diffusely immunoreactive with PTEN and its phosphorylated form in all groups, including the DEN-alone group. With regard to immunolocalization in association with GST-P-positive foci, a small population of GST-P-positive foci showed decreased PTEN expression, forming PTEN-negative foci, in the DEN-alone group. On the other hand, GST-P-positive foci induced by promotion with FB, PBO, or TAA also formed PTEN-negative foci with a significantly increased concordance ratio in GST-P-positive foci compared with the DEN-alone group; FB promotion attained the highest ratio (Fig. 1a). Similarly, phosphorylated PTEN also showed significantly decreased expression in GST-P-positive foci in proportion with the magnitude of the promotion by each chemical compared with the DEN-alone group (Fig. 1b).

Akt1, Akt2, and Akt3, as well as phospho-Akt (Ser473), did not show specific immunolocalization in the liver in any group. On the other hand, as with weak and diffuse immunoreactivity in the liver cells not forming cellular foci, enhanced expression of phospho-Akt2, forming phospho-Akt2-positive foci, was observed in a subpopulation of GST-P-positive foci in the livers of rats treated with DEN-alone (Fig. 2a). Co-expression with GST-P-positive foci was increased by promotion with FB, PBO, and TAA, with a statistically significant concordance ratio in GST-P-positive foci compared with the DEN-alone group; FB promotion attained the highest ratio (Fig. 2a).

Most foci positive for phospho-Akt2 were negative for PTEN. Figure 3 shows concordance ratios of phospho-Akt2-immunoreactivity in PTEN-negative foci in each group. All of the tumor-promoted groups showed approximately 50% of concordance ratios. While DEN-alone group showed slightly low concordance ratio (33%), there was no statistical significance between the DEN-alone and tumor-promoted groups.

Molecule(s) immunoreacted with antiphospho-(Ser/Thr) Akt substrate antibody showed specific localization to the cellular membrane in accordance with GST-P-positive foci (Fig. 2b). The concordance ratio for GST-P-positive foci was significantly increased by promotion with FB, PBO, or TAA compared with that in the unpromoted cases (DEN-alone), showing a similar magnitude among chemicals (Fig. 2b). Most foci positive for phospho-Akt substrate were negative for PTEN. Nuclear immunoreactivity was also diffusely observed in liver cells without relation to GST-P-positive foci.

Among known Akt substrates, Raf1 and Synip did not show any specific immunolocalization in association with GST-P-positive foci. On the other hand, 14-3-3 was weakly positive in liver cells not forming altered foci, and enhanced expression was observed in the small population of GST-P-positive foci in the DEN-alone and PBO-promoted groups, showing a diffuse cytoplasmic expression pattern with scattered nuclear immunoreactivity. The concordance ratio with GST-P-positive foci between the two groups did not differ statistically (Fig. 2c). Grb10 also coexpressed in a small

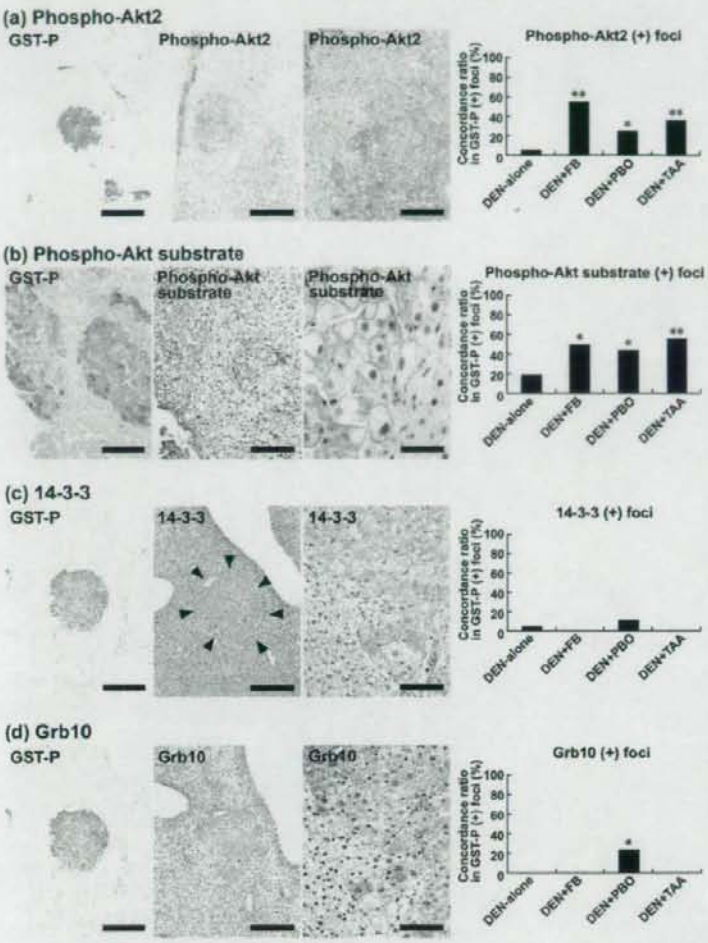

Fig. 2. Immunohistochemical localization of phospho-protein kinase B 2 (Akt2), phospho-Akt substrate, 14-3-3, and Grb10 (growth factor receptor bound protein 10) in glutathione *S*-transferase placental form (GST-P)-positive liver cell foci after promotion for 6 weeks. (a) Phospho-Akt2 expression (middle and right) in a GST-P-positive focus (left) in the liver of a rat promoted with 3600 p.p.m. fenbendazole (FB) after *N*-diethylnitrosamine (DEN) initiation. Note the mostly cytoplasmic expression with scattered nuclear immunoreactivity of phospho-Akt2. Bar = 500 μm (left and middle), 100 μm (right). The graph shows concordance ratios (%) of phospho-Akt2 immunoreactivity with GST-P-positive foci generated after promotion with FB, piperonyl butoxide (PBO), or thioacetamide (TAA). *, **: $P < 0.05$, 0.01 *versus* DEN-alone group (χ^2-test). (b) Immunoreactivity against antiphospho-Akt substrate antibody (middle and right) in a GST-P-positive focus (left) in the liver of a rat promoted with 400 p.p.m. TAA after DEN initiation. Note the predominant membrane immunoreactivity of phospho-Akt substrate. Bar = 100 μm (left and middle), 50 μm (right). The graph shows concordance ratios (%) of phospho-Akt substrate immunoreactivity with GST-P-positive foci generated after promotion with FB, PBO, or TAA. *, **: $P < 0.05$, 0.01 *versus* DEN-alone group (χ^2-test). (c) 14-3-3 expression (middle and right) in a GST-P-positive focus (left) in the liver of a rat promoted with 20 000 p.p.m. PBO after DEN initiation. Margin of the focus expressing 14-3-3 is marked with arrowheads (middle). Note both of the nuclear and cytoplasmic immunoreactivities of 14-3-3. Bar = 500 μm (left and middle), 100 μm (right). The graph shows concordance ratios (%) of 14-3-3 immunoreactivity with GST-P-positive foci generated after promotion with FB, PBO, or TAA. (d) Grb10 expression (middle and right) in a GST-P-positive focus (left) in the liver of a rat promoted with 20 000 p.p.m. PBO after DEN initiation. The same focus expressing 14-3-3 as shown in panel (c) is presented. Note both of the nuclear and cytoplasmic immunoreactivities of Grb10. Bar = 500 μm (left and middle), 100 μm (right). The graph shows concordance ratios (%) of Grb10 immunoreactivity with GST-P-positive foci generated after promotion with FB, PBO, or TAA. *: $P < 0.05$ *versus* DEN-alone group (χ^2-test).

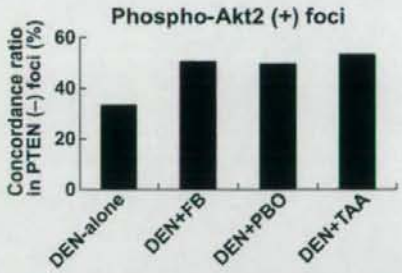

Fig. 3. Concordance ratios of phospho-protein kinase B 2 (Akt2) immunoreactivity with liver cell foci negative for phosphatase and tensin homolog deleted on chromosome 10 (PTEN) after promotion for 6 weeks with fenbendazole (FB), piperonyl butoxide (PBO), or thioacetamide (TAA).

population of GST-P-positive foci only in the PBO-promoted group, with a mainly cytoplasmic expression pattern and a statistically significant difference from the DEN-alone group (Fig. 2d).

TGFβRI showed diffuse but weak immunoreactivity in the liver cells not forming cellular foci in all groups, including the DEN-alone group. Populations of GST-P-positive foci in the livers of rats treated with DEN-alone did not form TGFβRI-positive foci (Fig. 4a). In contrast, coexpression of TGFβRI in GST-P-positive foci was apparent after promotion with FB, PBO, and TAA, with a statistically significant increase in the concordance ratio as compared with the DEN-alone group. The highest concordance ratio was attained with FB promotion (Fig. 4a).

Liver cells other than those consisting of GST-P-positive foci were diffusely immunoreactive with EGFR in all groups, including the DEN-alone group. With regard to the immunoreactivity in GST-P-positive foci, a small population showed decreased EGFR expression, forming EGFR-negative foci, in the DEN-alone group. On the other hand, EGFR-negative foci induced by promotion with FB, PBO, or TAA significantly increased the concordance ratio in GST-P-positive foci as compared with the DEN-alone group; TAA promotion showed the highest concordance ratio (Fig. 4b). The receptor molecules c-erbB2 and IGF-IRβ did not show any specific expression pattern in association with GST-P-positive foci in any group.

Liver polypeptide signal levels during the early stage of tumor promotion. Although numbers of animals examined were two in each group, increased band intensity of polypeptide of GST-P, phospho-Akt2, and TGFβRI was observed in the liver

doi: 10.1111/j.1349-7006.2009.01120.x

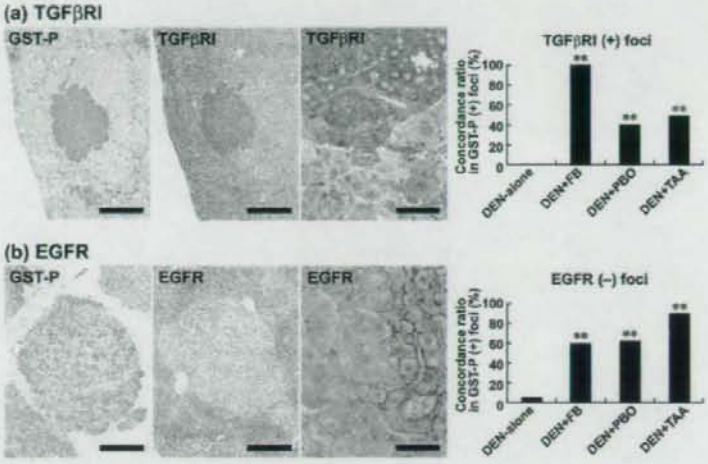

Fig. 4. Immunohistochemical localization of transforming growth factor-β receptor I (TGFβRI) and epidermal growth factor receptor (EGFR) in glutathione *S*-transferase placental form (GST-P)-positive liver cell foci after promotion for 6 weeks. (a) TGFβRI expression (middle and right) in a GST-P-positive focus (left) in the liver of a rat promoted with 3600 p.p.m. fenbendazole (FB) after *N*-diethylnitrosamine (DEN) initiation. Note the mostly cytoplasmic expression of TGFβRI. Bar = 500 μm (left and middle), 50 μm (right). The graph shows the concordance ratios (%) of TGFβRI immunoreactivity with GST-P-positive foci generated after promotion with FB, piperonyl butoxide (PBO), or thioacetamide (TAA). **: $P < 0.01$ *versus* DEN-alone group (χ^2-test). (b) Lack of EGFR expression (middle and right) in a GST-P-positive focus (left) in the liver of a rat promoted with 3600 p.p.m. FB after DEN initiation. Bar = 500 μm (left and middle), 50 μm (right). The graph shows the concordance ratios (%) of EGFR negativity with GST-P-positive foci generated after promotion with FB, PBO, or TAA. **: $P < 0.01$ *versus* DEN-alone group (χ^2-test).

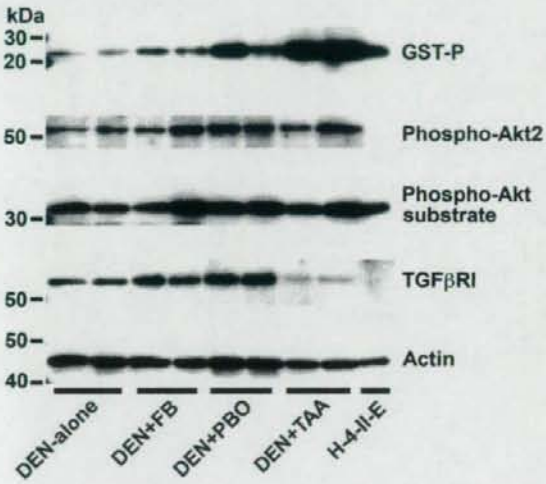

Fig. 5. Polypeptide signal levels of glutathione *S*-transferase placental form (GST-P), phospho-protein kinase B 2 (Akt2), phospho-Akt substrate, and transforming growth factor-β receptor I (TGFβRI) in the liver tissues after promotion for 6 weeks (N = 2/group). Blotted membranes were prepared for signal detection of each antigen and reprobed with actin as a control for sample loading. Cell lysate of a rat hepatoma cell line that is known to express GST-P, H-4-II-E, was also included in the analysis. As compared with *N*-diethylnitrosamine (DEN)-alone group, mean relative values of band intensity of GST-P are 1.7 by promotion with fenbendazole (FB), 5.8 with piperonyl butoxide (PBO), and 13.8 with thioacetamide (TAA). With regard to phospho-Akt2, relative values as compared with DEN-alone group are 1.4 by promotion with FB, 2.0 with PBO, and 1.7 with TAA. With regard to phospho-Akt substrate, a single band migrating approximately 32 kDa could be detected in all groups, and relative values to DEN-alone group are 1.3 by promotion with FB, 1.5 with PBO, and 1.3 with TAA. Relative levels of TGFβRI signal as compared to DEN-alone group are 1.5 by promotion with FB, 2.2 with PBO, and 0.2 with TAA. Relative levels of actin signal to the DEN-alone group as represented by the samples examined for TGFβRI expression shown here are 0.8 by promotion with FB, 1.1 with PBO, and 0.7 with TAA.

after promotion with FB, PBO, or TAA, except for the reduction of TGFβRI signal with TAA-promotion (Fig. 5). With regard to phospho-Akt substrate, a single band migrating approximately 32 kDa could be detected in all groups including DEN-alone group, and increase of this signal was evident in the liver by promotion with FB, PBO, or TAA.

Immunolocalization during the late stage of tumor promotion. Many adenomas and carcinomas were obtained after promotion by FB for 57 weeks.[13] The adenomas often exhibited eosinophilic cytoplasm and solid growth, and the carcinomas frequently showed island and solid growth patterns. Foci observed at the late stage were mostly eosinophilic, but rarely, basophilic cell types were found.

All adenomas and carcinomas were positive for GST-P, although a small subset of foci, such as the basophilic type, appeared negative. The numbers of liver cell foci, adenomas, and carcinomas showing GST-P-immunoreactivity and subjected to further immunohistochemical analyses were 61, 24, and 9, respectively.

Akt1, Akt2, and Akt3, as well as phospho-Akt (Ser473), did not show specific immunolocalization in association with GST-P-positive lesions. On the other hand, localized expression of phospho-Akt2 was observed in the liver cell foci and neoplastic lesions, and the concordance ratio of this immunolocalization with GST-P immunoreactivity was increased in association with lesion development from foci to carcinomas (Figs 6a,b and 7). All of the nine carcinomas examined showed positive immunolocalization of phospho-Akt2.

With regard to the distribution of molecule(s) immunoreacted with antiphospho-(Ser/Thr) Akt substrate antibody, lesion-specific immunoreactivity was increased in association with lesion development from foci to carcinomas, reflecting the concordance ratio with GST-P immunoreactivity (Figs 6c,d and 7). Regarding subcellular localization, liver cell foci showed immunolocalization either at the cell surface membrane or in the cytoplasm. Adenomas showed three types of localization, i.e. cell membrane alone, cytoplasm alone, and both membrane and cytoplasm. The ratio of adenomas showing only cytoplasmic expression was increased compared with hepatocellular foci. All carcinomas examined showed a cytoplasmic immunolocalization pattern. Weak nuclear immunoreactivity was also observed in the liver cells without showing specific immunolocalization to foci or neoplastic lesions.

With regard to TGFβRI immunoexpression, the concordance ratio with GST-P immunoreactivity was rather high in all types of lesions (Figs 6e and 7). Decreased EGFR expression was observed in almost all of the GST-P-positive proliferative lesions from foci to carcinomas (Figs 6f and 7). Other RTKs, c-erbB2, and IGF-IRβ, as well as 14-3-3 and Grb10, did not show any specific expression pattern in association with proliferative lesions.

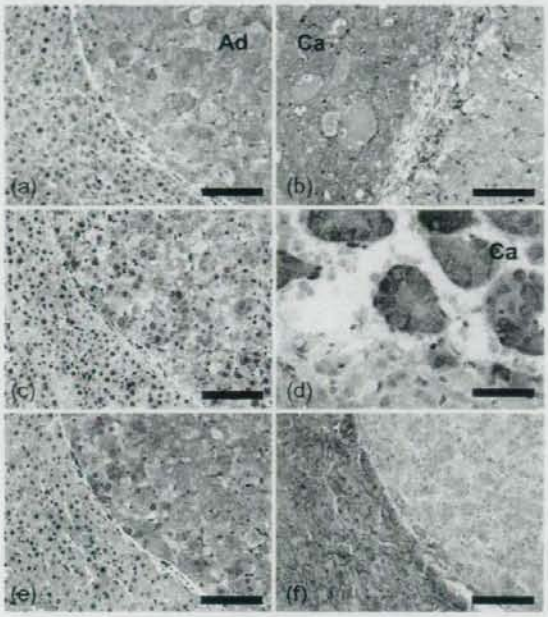

Fig. 6. Immunolocalization of phospho-protein kinase B 2 (Akt2), phospho-Akt substrate, transforming growth factor-β receptor I (TGFβRI), and epidermal growth factor receptor (EGFR) in the glutathione *S*-transferase placental form-positive proliferative lesions generated after promotion by fenbendazole for 57 weeks. (a,b) Selective expression of phospho-Akt2 in an adenoma (a) and in a carcinoma (b) in contrast to surrounding non-tumor tissue. (c,d) An adenoma showing both cytoplasmic and membrane immunoreactivities (c), and a carcinoma showing predominantly cytoplasmic immunoreactivity (d) with the antibody against phospho-Akt substrate. (e,f) Positive immunoreactivity of TGFβRI (e) and negative reactivity of EGFR (f) in an adenoma. Immunoreactivity in the same portion of the identical adenoma is presented in panels (a), (c), (e), and (f). (a), (b), (c), (e), (f) Bar = 100 μm (d) Bar = 50 μm. Ad, adenoma; Ca, carcinoma.

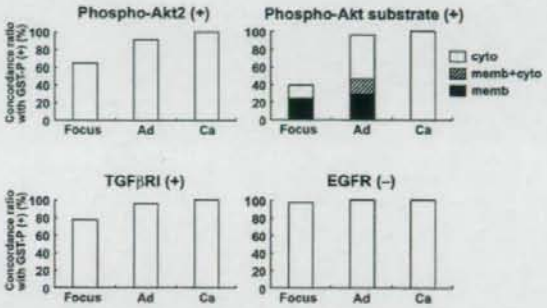

Fig. 7. The concordance ratios (%) of the immunoreactive proliferative lesions for phospho-protein kinase B 2 (Akt2), phospho-Akt substrate, and transforming growth factor-β receptor I (TGFβRI), and negative foci for epidermal growth factor receptor (EGFR) in the glutathione *S*-transferase placental form (GST-P)-positive proliferative lesions produced after promotion by fenbendazole for 57 weeks. Ad, adenoma; Ca, carcinoma; cyto, cytoplasm; memb, membrane.

Discussion

Our previous study demonstrated down-regulation of PTEN expression, including its inactive phosphorylated form, in a majority of altered liver cell foci generated by tumor promotion in the early stage.[13] Here, we investigated the cellular localization of molecules involved in Akt signaling that are negatively regulated by PTEN in GST-P-positive preneoplastic lesions at the early stage of promotion. As a result, we found an increase in the ratios of GST-P-positive foci coexpressing phospho-Akt2 and the undetermined downstream substrate molecule(s) of Akt-kinase activity in the promoted cases. Further, most of phospho-Akt2-positive foci and phospho-Akt substrate-positive foci were found in subpopulations of PTEN-negative foci. On the other hand, total phosphorylated and non-phosphorylated forms of Akt1, Akt2, and Akt3, as well as phospho-Akt did not show any specific localization in association with liver cell foci. These results suggest an enhanced activation of Akt2 in response to promotion stimuli in subpopulations of GST-P-positive foci to show lack of PTEN-expression. GST-P-positive foci also showed up-regulation of TGFβRI and down-regulation of EGFR in response to tumor promotion with hepatocarcinogens. Although the possibility of chemical-dependent response remains to be addressed, these results suggest a crosstalk between the TGFβ and PTEN/Akt2 signaling cascades, involving a mechanism to cause EGFR down-regulation by promotion at the early stage. A similar pattern of cellular distribution of these molecules was observed in the neoplastic lesions at the late stage, suggesting these are essential molecular events in the entire process of tumor promotion.

The *AKT2* gene product is strongly correlated with the regulation of glucose homoeostasis and is the predominant Akt isoform expressed in insulin-responsive tissues.[28] Akt2 has also been implicated in human malignancies, and recently, Akt2 has been shown to regulate cancer cell survival, migration, and invasion, acting as a transcriptional regulatory target of the basic helix-loop-helix transcriptional factor Twist.[29] In the present study, among Akt isoforms, we could only detect increased coexpression of the activated form, phospho-Akt2, in subpopulations of GST-P-positive foci induced by tumor promotion. Increase in the polypeptide level of phospho-Akt2 was also observed in the liver of tumor-promoted cases. The following phenomena may underlie the mechanisms for clonal expansion of GST-P-positive cells: lack of a p53 response to DNA damage because of transactivation of *Mdm2* oncogene,[4,5] down-regulation of apoptosis,[6,30] and up-regulation of cell proliferation.[31] Although the direct evidence for the functional relevance of active Akt2 in GST-P-positive foci needs to be clarified, Akt, once phosphorylated and activated, is known to relocalize to several subcellular locations where it phosphorylates proteins, such as Forkhead transcription factors, glycogen synthesis kinase-3, Bcl2-antagonist of cell death, and Mdm2 – some of which contribute to antiapoptotic signaling.[32]

In this study, we also found membrane localization of molecule(s) immunoreactive with antiphospho-(Ser/Thr) Akt substrate antibody in the GST-P-positive preneoplastic lesions at 6 weeks of tumor promotion. To identify the corresponding molecule, we first examined the cellular localization of four candidates of Akt substrates that were selected because of reported cell surface membrane localization.[19–25] As a result, 14-3-3 and Grb10 showed increased cytoplasmic expression in a subpopulation of GST-P-positive foci induced only by promotion with PBO. We next examined polypeptide signal levels immunoreacted with the antiphospho-(Ser/Thr) Akt substrate antibody in the liver of tumor promoted cases. As a result, a single polypeptide signal, migrating approximately at 32 kDa, was detected in all groups, and enhanced expression was observed after tumor promotion. Interestingly, the pattern of immunolocalization changed from the membrane to the cytoplasm in relation with lesion development. All carcinomas showed cytoplasmic localization, suggesting an alteration of the function or activity of the corresponding molecule(s).

doi: 10.1111/j.1349-7006.2009.01120.x

TGFβ exerts a growth-inhibitory effect on epithelial cells, which explains its role as a tumor suppressor that cancer cells must elude for malignant evolution.[33] Yet, paradoxically, TGFβ also modulates processes such as cell invasion, immune regulation, and microenvironment modification that cancer cells may exploit to their advantage.[34] In our previous study, we found that TGFβRI was selectively expressed in proliferative lesions from early preneoplastic liver cell foci induced by promotion with PB or FB, whereas TGFβRII showed less selective expression in relation with proliferative lesions.[13] In the present study, we also found TGFβRI expression in subpopulations of GST-P-positive foci generated after promotion with PBO or TAA as well as FB, whereas no apparent immunoreactivity was found with GST-P-positive foci induced without any promotion. In parallel with the immunohistochemical results, polypeptide signal of TGFβRI was increased in the liver after promotion with FB or PBO. TAA-promoted cases, on the other hand, decreased the polypeptide signal, in contrast to the increased expression in the preneoplastic liver cell foci. In the immunohistochemical analysis of focal strong expression as in the present study, weak constitutive expression is usually excluded from the evaluation of immunohistochemical results. However, constitutive expression could be detected by immunoblot analysis. Therefore, although the reason for the discrepancy in the result between the immunohistochemistry and immunoblotting was not clear, difference in the constitutively expressed level of TGFβRI in liver cells not forming preneoplastic foci between groups including DEN-alone group might be involved.

Considering the similarity of the immunolocalization pattern of TGFβRI with the above-examined PTEN/Akt signaling molecules, some signal crosstalk may occur between TGFβ and PTEN/Akt signaling for formation of preneoplastic lesions under tumor-promoting stimuli. TGFβ has been shown to induce transcriptional down-regulation of PTEN in neoplastic cells, suggesting a role for TGFβ signaling in their growth promotion.[35] It has also been reported that activation of Akt is required for TGFβ-mediated cell survival, epithelial-to-mesenchymal transition, and cell migration.[36,37] This activation can result from TGFβ-induced TGF-α expression and consequent EGF-receptor activation.[37] According to our previous study results, populations of PTEN-negative proliferative lesion were slightly but consistently larger than TGFβRI-positive ones at both early and late stages of tumor promotion by FB and PB,[13] suggesting an acquisition of TGFβ signaling in a subpopulation of PTEN-negative lesions. On the other hand, in the analysis of the present study, GST-P-positive neoplastic lesions at the late stage of tumor promotion by FB showed higher concordance ratios with Akt2, phospho-Akt substrate, and TGFβRI, than GST-P-positive liver cell foci. Most of these neoplastic lesions expressed above all molecules. These results suggest that crosstalk between TGFβ and PTEN/Akt signaling plays a role for the development of neoplastic lesions as an outcome of tumor promotion.

EGFR is a c-erbB family protein that can heterodimerize for ligand-dependent activation of downstream signaling. Interestingly, selective down-regulation of EGFR in a majority of GST-P-positive foci was observed at 6 weeks of promotion in the present study, while c-erbB2 did not show any specific expression pattern. Moreover, most of the GST-P-positive proliferative lesions, including carcinomas presented here, also down-regulated EGFR at the later stage. It is well known that EGFR can be down-regulated in a ligand-dependent manner because of internalization and the following efficient degradation, resulting in a dramatic decrease in the half-life of the EGFR protein,[38] and long-term down-regulation of receptor activity can occur through this mechanism.[39] This type of EGFR down-regulation can occur via clathrin-dependent or independent mechanisms; activity of PI3K as well as that of EGFR kinase and dynamin would be required for the latter.[40] Another possibility for the mechanism underlying selective down-regulation of EGFR is transcriptional gene silencing by CpG island hypermethylation.[41] Although further studies are needed to examine whether EGFR is activated or inactivated in the GST-P-positive foci and neoplastic cells, TGFβ activates survival signals such as Akt, and EGFR is required for its activation.[42] A subpopulation of GST-P-positive liver cell foci expresses TGFα, acting as a c-erbB ligand.[43]

In summary, we found an enhanced activation of PTEN/Akt2 signaling in preneoplastic and neoplastic lesions in response to tumor promotion from the early stages of hepatocarcinogenesis. Considering the up-regulation of TGFβRI and down-regulation of EGFR in relation with PTEN/Akt2 in these lesions, there is likely crosstalk between Akt2 and TGFβ signaling, involving a mechanism requiring EGFR down-regulation during the entire process of tumor promotion starting from the early stage.

Acknowledgments

We thank Mrs Sumiko Hayashi for her technical assistance in analysis of immunoblotting. This work was supported by Health and Labour Sciences Research Grants (Research on Food Safety) from the Ministry of Health, Labour and Welfare of Japan.

References

1 Shirai T. A medium-term rat liver bioassay as a rapid in vivo test for carcinogenic potential, a historical review of model development and summary of results from 291 tests. *Toxicol Pathol* 1997; **25**: 453–60.
2 Ito N, Imaida K, Asamoto M, Shirai T. Early detection of carcinogenic substances and modifiers in rats. *Mutat Res* 2000; **462**: 209–17.
3 Miller RT, Cattley RC, Marsman DS, Lyght O, Popp JA. TGFα differentially expressed in liver foci induced by diethylnitrosamine initiation and peroxisome proliferator promotion. *Carcinogenesis* 1995; **16**: 77–82.
4 Van Gijssel HE, Ohlson LC, Torndal UB *et al.* Loss of nuclear p53 protein in preneoplastic rat hepatocytes is accompanied by Mdm2 and Bcl-2 overexpression and by defective response to DNA damage *in vivo*. *Hepatology* 2000; **32**: 701–10.
5 Finnberg N, Silins I, Stenius U, Högberg J. Characterizing the role of MDM2 in diethylnitrosamine induced acute liver damage and development of pre-neoplastic lesions. *Carcinogenesis* 2004; **25**: 113–22.
6 Ogawa K, Asamoto M, Suzuki S, Tsujimura K, Shirai T. Downregulation of apoptosis revealed by laser microdissection and cDNA microarray analysis of related genes in rat liver preneoplastic lesions. *Med Mol Morph* 2005; **38**: 23–9.
7 Vanhaesebroeck B, Alessi DR. The PI3K-PDK1 connection: more than just a road to PKB. *Biochem J* 2000; **346**: 561–76.
8 Maehama T, Taylor GS, Dixon JE. PTEN and myotubularin: novel phosphoinositide phosphatases. *Annu Rev Biochem* 2001; **70**: 247–79.
9 West KA, Castillo SS, Dennis PA. Activation of the PI3K/Akt pathway and chemotherapeutic resistance. *Drug Resist Updat* 2002; **5**: 234–48.
10 Brader S, Eccles SA. Phosphoinositide 3-kinase signalling pathways in tumor progression, invasion and angiogenesis. *Tumori* 2004; **90**: 2–8.
11 Datta SR, Brunet A, Greenberg ME. Cellular survival: a play in three Akts. *Genes Dev* 1999; **13**: 2905–27.
12 Silins I, Högberg J, Stenius U. Dietary sphingolipids suppress a subset of preneoplastic rat liver lesions exhibiting high PTEN, low phospho-Akt and high levels of ceramide species. *Food Chem Toxicol* 2006; **44**: 1552–61.
13 Takahashi M, Shibutani M, Woo GH *et al.* Cellular distributions of molecules with altered expression specific to the tumor promotion process from the early stage in a rat two-stage hepatocarcinogenesis model. *Carcinogenesis* 2008; **29**: 2218–26.
14 Zhang H, Bajraszewski N, Wu E *et al.* PDGFRs are critical for PI3K/Akt activation and negatively regulated by mTOR. *J Clin Invest* 2007; **117**: 730–8.
15 Murillo MM, del Castillo G, Sánchez A, Fernández M, Fabregat I. Involvement of EGF receptor and c-Src in the survival signals induced by TGF-beta1 in hepatocytes. *Oncogene* 2005; **24**: 4580–7.
16 Shoda T, Onodera H, Takeda M *et al.* Liver tumor promoting effects of fenbendazole in rats. *Toxicol Pathol* 1999; **27**: 553–62.
17 Muguruma M, Unami A, Kanki M *et al.* Possible involvement of oxidative stress in piperonyl butoxide induced hepatocarcinogenesis in rats. *Toxicology* 2007; **236**: 61–75.
18 Kuroda K, Terao K, Akao M. Inhibitory effect of fumaric acid on hepatocarcinogenesis by thioacetamide in rats. *J Natl Cancer Inst* 1987; **79**: 1047–51.

19 Shikano S, Coblitz B, Wu M, Li M. 14-3-3 proteins: regulation of endoplasmic reticulum localization and surface expression of membrane proteins. *Trends Cell Biol* 2006; **16**: 370–5.
20 Powell DW, Rane MJ, Chen Q, Singh S, McLeish KR. Identification of 14-3-3ζ as a protein kinase B/Akt substrate. *J Biol Chem* 2002; **277**: 21639–42.
21 Kebache S, Ash J, Annis MG *et al.* Grb10 and active Raf-1 kinase promote Bad-dependent cell survival. *J Biol Chem* 2007; **282**: 21873–83.
22 Jahn T, Seipel P, Urschel S, Peschel C, Duyster J. Role for the adaptor protein Grb10 in the activation of Akt. *Mol Cell Biol* 2002; **22**: 979–91.
23 Goetz CA, O'Neil JJ, Farrar MA. Membrane localization, oligomerization, and phosphorylation are required for optimal raf activation. *J Biol Chem* 2003; **278**: 51184–9.
24 Kao G, Tuck S, Baillie D, Sundaram MVC. elegans SUR-6/PR55 cooperates with LET-92/protein phosphatase 2A and promotes Raf activity independently of inhibitory Akt phosphorylation sites. *Development* 2004; **131**: 755–65.
25 Yamada E, Okada S, Saito T *et al.* Akt2 phosphorylates Synip to regulate docking and fusion of GLUT4-containing vesicles. *J Cell Biol* 2005; **168**: 921–8.
26 Lee KY, Shibutani M, Inoue K *et al.* Methacarn fixation – effects of tissue processing and storage conditions on detection of mRNAs and proteins in paraffin-embedded tissues. *Anal Biochem* 2006; **351**: 36–43.
27 Ikeda H, Nishi S, Sakai M. Transcription factor Nrf2/MafK regulates rat placental glutathione *S*-transferase gene during hepatocarcinogenesis. *Biochem J* 2004; **380**: 515–21.
28 Dummler B, Hemmings BA. Physiological roles of PKB/Akt isoforms in development and disease. *Biochem Soc Trans* 2007; **35**: 231–5.
29 Cheng GZ, Zhang W, Wang LH. Regulation of cancer cell survival, migration, and invasion by Twist: AKT2 comes to interplay. *Cancer Res* 2008; **68**: 957–60.
30 Luebeck EG, Buchmann A, Stinchcombe S, Moolgavkar SH, Schwarz M. Effects of 2,3,7,8-tetrachlorodibenzo-*P*-dioxin on initiation and promotion of GST-P-positive foci in rat liver: A quantitative analysis of experimental data using a stochastic model. *Toxicol Appl Pharmacol* 2000; **167**: 63–73.
31 Kinoshita A, Wanibuchi H, Morimura K *et al.* Phenobarbital at low dose exerts hormesis in rat hepatocarcinogenesis by reducing oxidative DNA damage, altering cell proliferation, apoptosis and gene expression. *Carcinogenesis* 2003; **24**: 1389–99.
32 Woodgett JR. Recent advances in the protein kinase B signaling pathway. *Curr Opin Cell Biol* 2005; **17**: 150–7.
33 Derynck R, Zhang YE. Smad-dependent and Smad-independent pathways in TGF-β family signalling. *Nature* 2003; **425**: 577–84.
34 Massagué J. TGFβ in cancer. *Cell* 2008; **134**: 215–30.
35 Chow JY, Quach KT, Cabrera BL, Cabral JA, Beck SE, Carethers JM. RAS/ERK modulates TGFβ-regulated PTEN expression in human pancreatic adenocarcinoma cells. *Carcinogenesis* 2007; **28**: 2321–7.
36 Bakin AV, Tomlinson AK, Bhowmick NA, Moses HL, Arteaga CL. Phosphatidylinositol 3-kinase function is required for transforming growth factor β-mediated epithelial to mesenchymal transition and cell migration. *J Biol Chem* 2000; **275**: 36803–10.
37 Vinals F, Pouysségur J. Transforming growth factor β1 (TGF-β1) promotes endothelial cell survival during in vitro angiogenesis via an autocrine mechanism implicating TGF-α signaling. *Mol Cell Biol* 2001; **21**: 7218–30.
38 Sorkin A, Goh LK. Endocytosis and intracellular trafficking of ErbBs. *Exp Cell Res* 2008; **314**: 3093–106.
39 Sorkin A, Waters CM. Endocytosis of growth factor receptors. *Bioessays* 1993; **15**: 375–82.
40 Orth JD, Krueger EW, Weller SG, McNiven MA. A novel endocytic mechanism of epidermal growth factor receptor sequestration and internalization. *Cancer Res* 2006; **66**: 3603–10.
41 Montero AJ, Díaz-Montero CM, Mao L *et al.* Epigenetic inactivation of EGFR by CpG island hypermethylation in cancer. *Cancer Biol Ther* 2006; **5**: 1494–501.
42 Caja L, Ortiz C, Bertran E *et al.* Differential intracellular signaling induced by TGF-β in rat adult hepatocytes and hepatoma cells: Implications in liver carcinogenesis. *Cell Signal* 2007; **19**: 683–94.
43 Kitano M, Ichihara T, Matsuda T *et al.* Presence of a threshold for promoting effects of phenobarbital on diethylnitrosamine-induced hepatic foci in the rat. *Carcinogenesis* 1998; **19**: 1475–80.

doi: 10.1111/j.1349-7006.2009.01120.x

Cellular distributions of molecules with altered expression specific to thyroid proliferative lesions developing in a rat thyroid carcinogenesis model

Gye-Hyeong Woo,[1] Miwa Takahashi,[1] Kaoru Inoue,[1] Hitoshi Fujimoto,[1] Katsuhide Igarashi,[2] Jun Kanno,[2] Masao Hirose,[1,3] Akiyoshi Nishikawa[1] and Makoto Shibutani[1,4,5]

Divisions of [1]Pathology, [2]Molecular Toxicology, National Institute of Health Sciences, Setagaya-ku, Tokyo; [3]Food Safety Commission, Chiyoda-ku, Tokyo; [4]Laboratory of Veterinary Pathology, Tokyo University of Agriculture and Technology, Fuchu-shi, Tokyo, Japan

(Received November 15, 2008/Revised December 25, 2008/Accepted December 26, 2008/Online publication February 26, 2009)

To identify differentially regulated molecules related to early and late stages of tumor promotion in a rat two-stage thyroid carcinogenesis model by an antithyroid agent, sulfadimethoxine, microarray-based microdissected lesion-specific gene expression profiling was carried out. Proliferative lesions for profiling were divided into two categories: (i) focal follicular cell hyperplasias (FFCH) and adenomas (Ad) as early lesions; and (ii) carcinomas (Ca) as more advanced. In both cases, gene expression was compared with that in surrounding non-tumor follicular cells. Characteristically, upregulation of cell cycle-related genes in FFCH + Ad, downregulation of genes related to tumor suppression and transcription inhibitors of inhibitor of DNA binding (Id) family proteins in Ca, and upregulation of genes related to cell proliferation and tumor progression in common in FFCH + Ad and Ca, were detected. The immunohistochemical distributions of molecules included in the altered expression profiles were further examined. In parallel with microarray data, increased localization of ceruloplasmin, cyclin B1, and cell division cycle 2 homolog A, and decreased localization of poliovirus receptor-related 3 and Id3 were observed in all types of lesion. Although inconsistent with the microarray data, thyroglobulin immunoreactivity appeared to reduce in Ca. The results thus suggest cell cycling facilitation by induction of M-phase-promoting factor consisting of cyclin B1 and cell division cycle 2 homolog A and generation of oxidative responses as evidenced by ceruloplasmin accumulation from an early stage, as well as suppression of cell adhesion involving poliovirus receptor-related 3 and inhibition of cellular differentiation regulated by Id3. Decrease of thyroglobulin in Ca may reflect dedifferentiation with progression. (*Cancer Sci* 2009; 100: 617–625)

Although clinically recognized thyroid Ca constitute less than 1% of all human malignant tumors, it is the most common endocrine cancer (90% of cases) and is responsible for more deaths than all other endocrine cancers combined.[1] Ca of the thyroid is usually of follicular cell origin, but the medullary carcinoma arises from parafollicular or C cells. In humans, causative factors for thyroid Ca are not well understood except for secondary occurrence after radiotherapy.[2] In rats, on the other hand, thyroid follicular cell tumors can be produced by administration of antithyroid agents, such as by propylthiouracil,[3] methimazole,[4] and 3-amino-1,2,4-triazole,[5] in an initiation-promotion model.

Many chemicals that can induce thyroid tumors in rodents cause disruption of the thyroid–pituitary axis through induction of hypothyroidism.[6] The putative mechanism for this carcinogenesis is believed to be non-genotoxic, decrease in the serum levels of triiodothyronine and thyroxine causing suppression of negative feedback through the pituitary and an increase in serum TSH. TSH then stimulates thyroid functions, including growth and proliferation of follicular cells.[7,8] However, detailed molecular mechanisms remain to be resolved.[6]

SDM is a broad-spectrum antimicrobial sulfonamide that has been shown to effectively induce thyroid follicular cell tumors in a rat two-stage thyroid carcinogenesis model after initiation with DHPN.[9] The anti-thyroidal effects of this drug are mediated through inhibition of iodination reactions catalyzed by thyroid peroxidase, resulting in reduction of thyroid hormone synthesis and increased levels of TSH in the bloodstream.[10]

Histological lesion-specific gene expression profiling provides valuable information on the mechanisms underlying lesion development. We have established molecular analysis methods for DNA, RNA, and proteins in paraffin-embedded small-tissue specimens utilizing an organic solvent-based fixative, methacarn,[11–13] and applied them for analyses of microdissected lesions.[14,15] With regard to mRNA expression analysis, expression fidelity in the methacarn-fixed paraffin-embedded tissues was found to be very close to that in the unfixed frozen tissues in both the real-time RT-PCR and oligonucleotide microarray systems, suggesting a great advantage of methacarn in analyses of microdissected lesions after paraffin embedding.[14,15]

In the present study, to identify differentially regulated molecules related to thyroid carcinogenesis through hypothyroidism, we carried out global gene expression profiling of early and late-stage proliferative lesions obtained after promotion with SDM in a rat two-stage carcinogenesis model. Localization of representative molecules showing altered expression was further analyzed immunohistochemically.

Materials and Methods

Chemicals and animals. DHPN (CAS no. 53609-64-6) and SDM (CAS no. 122-11-2) were purchased from Nacalai Tesque (Kyoto, Japan) and Sigma (St Louis, MO, USA), respectively. Male 5-week-old F344 rats were purchased from Japan SLC (Hamamatsu, Japan) and housed four to five rats per polycarbonate cage with sterilized softwood chips as bedding in a barrier-sustained animal room conditioned at 24 ± 1°C and 55 ± 5% humidity, with a 12:12 h L : D cycle. They received CRF-1 (Oriental Yeast Co., Tokyo, Japan) as a basal diet and water *ad libitum* throughout the experimental period, including the 1 week of acclimation.

Experimental design. At 6 weeks of age, 30 rats were injected subcutaneously with 2800 mg/kg body weight DHPN. Another

[5]To whom correspondence should be addressed. E-mail: mshibuta@cc.tuat.ac.jp

Abbreviations: Ad, adenoma; Ca, carcinoma; Ccnb1, cyclin B1; Cdc2, cell division cycle 2; DHPN, *N*-bis(2-hydroxypropyl)nitrosamine; FFCH, focal follicular cell hyperplasia; Id, inhibitor of DNA binding; IGSF, immunoglobulin superfamily; NTF, non-tumor follicles; PCR, polymerase chain reaction; Pvrl3, poliovirus receptor-related 3; RT, reverse transcription; SDM, sulfadimethoxine; TSH, thyroid-stimulating hormone.

doi: 10.1111/j.1349-7006.2009.01094.x

group of nine animals was injected with the vehicle saline as non-treated controls. One week later, 25 DHPN-initiated animals were administered SDM at 1000 p.p.m. in the drinking water *ad libitum* for up to 15 weeks. The other five DHPN-initiated animals were maintained on tap water for 10 weeks as a DHPN-alone group. At week 10 after SDM treatment, 10 animals were killed for microdissection of FFCH + Ad as well as NTF in each animal. The other SDM-promoted animals were further maintained until week 15, when 12 rats were killed for microdissection of Ca. Five untreated controls and the DHPN-alone group were killed at week 10 of SDM promotion, and the four remaining untreated controls at week 15. All animals were killed by exsanguination from the abdominal aorta under deep anesthesia with ether. The animal protocol was reviewed and approved by the Animal Care and Use Committee of the National Institute of Health Sciences, Japan.

Preparation of tissue specimens and microdissection. Caudal halves of the bilateral thyroid tissues of SDM-promoted animals were immersed in methacarn solution for 2 h at 4°C.[11] Tissue samples were then dehydrated, immersed in xylene, and embedded in paraffin as described previously.[15] Embedded tissue blocks were stored at 4°C until microdissection.[16]

For microarray analysis, 4 μm-thick sections between 10 16 μm-thick serial sections were prepared. The 16 μm-thick sections were mounted onto PEN-foil film (Leica Microsystems, Welzlar, Germany) overlaid on glass slides, dried in an incubator overnight at 37°C, and then stained using an LCM staining kit (Ambion, Austin, TX, USA). All microdissections were carried out within 2 h of tissue staining. The histopathological identity of each FFCH, Ad, and Ca, as well as NTF, was determined under microscopic observation of the adjacent 4 μm-thick sections stained with hematoxylin–eosin according to published criteria (Fig. 1).[17] In the present carcinogenesis model with SDM promotion, capsular invasive carcinomas are generated in addition to less-frequent parenchymal Ca.[18] In the present study, parenchymal proliferative lesions including the latter were subjected to laser microbeam microdissection (Leica Microsystems). Approximately 20 sections of bilateral thyroids were subjected to microdissection in one animal, and the microdissected samples (NTF, FFCH + Ad, and Ca) were collected and stored in separate 1.5-mL sample tubes at –80°C until extraction of total RNA.

RNA isolation, amplification, and microarray analysis. Total RNA extraction from each histological sample and quantitation of the RNA yield were carried out according to methods described previously.[15]

For microarray analysis, equal amounts of extracted total RNA samples from two animals were mixed (100 ng/sample) and subjected to amplification, consisting of RT and subsequent two-step *in vitro* transcription, using a MessageAmp II aRNA Kit (Ambion).

Second-round-amplified biotin-labeled antisense RNA was subjected to hybidization with a GeneChip Rat Genome 230 2.0 Array (Affymetrix Inc., Santa Clara, CA, USA). RNA samples collected from two animals were subjected to analysis with individual microarrays (n = 5/histological preparation).

Selection of genes and normalization of expression data were carried out using GeneSpring software (ver7.2; Silicon Genetics, Redwood City, CA, USA). To normalize chip-wide variation in intensity, per chip normalization was performed by dividing the signal strength for each gene with the level of the 50th percentile of the measurement in the chip, and dividing the value by the average intensity in the samples of NTF. Genes showing signals judged to be 'absent' in all 10 samples of NTF and each proliferative lesion group (FFCH + Ad or Ca) for comparison were excluded. Then, genes showing expression change with differences at least 2-fold in magnitude in the proliferative lesion groups from the NTF, as well as the 'presence' signal in more than four of five samples in the histological lesion group (NTF or each proliferative lesion group) showing higher expression values in comparison, were selected. Genes showing altered expression in common in both FFCH + Ad and Ca were also selected.

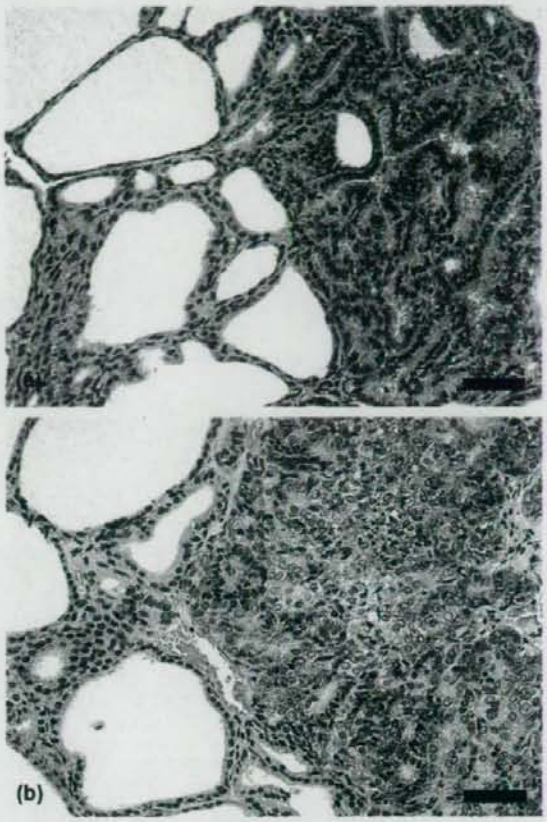

Fig. 1. Representative proliferative lesions developing after promotion with sulfadimethoxine (SDM) for (a) 10 or (b) 15 weeks in a rat two-stage thyroid carcinogenesis model. (a) Adenoma with follicular features, showing expansive growth with minor atypia. (b) Carcinoma showing obvious cellular atypia, consisting of follicular and solid growth elements with structural irregularity. Note focal necrosis and fibrosis. Hematoxylin–eosin staining. Scale bars = 50 μm.

Real-time RT-PCR. Quantitative real-time RT-PCR was carried out for confirmation of expression values obtained with microarrays using an ABI Prism 7900HT (Applied Biosystems, Foster City, CA, USA). The following 11 genes (eight upregulated and three downregulated in proliferative lesions) were selected as targets: chitinase 3-like 1, ceruloplasmin, solute carrier family 2 (facilitated glucose transporter) member 3, solute carrier family 16 (monocarboxylic acid transporters) member 6, glucagon, prolactin receptor, phosphatidylinositol 4-kinase type 2α, and actinin α1 as upregulated examples; and *Pvrl3*, retinoic acid induced 3, and glucosaminyl (*N*-acetyl) transferase 1 core 2 as downregulated examples. RT was carried out using first-round antisense RNA prepared for microarray analysis. Real-time PCR analysis of ceruloplasmin, glucagon, and glucosaminyl (*N*-acetyl) transferase 1 core 2 was carried out using ABI Assays-on-Demand TaqMan probe and primer sets from Applied Biosystems (available at https://products.appliedbiosystems.com/ab/en/US/

doi: 10.1111/j.1349-7006.2009.01094.x

Table 1. Sequences of primers used for real-time reverse transcription–polymerase chain reaction with the SYBR Green detection system

Gene	Accession no.	Sense/Antisense	Sequence
Chi3l1	AA945643	Sense	5′-TCGTTAACAGGGATGACCTGTATCT-3′
		Antisense	5′-GGGTAGGACGGTGGGATTGT-3′
Slc2a3	AA901341	Sense	5′-AAGCTGGCCATTGGCAAAT-3′
		Antisense	5′-CTAGCCTCTTGTGCTCCTCCAT-3′
Slc16a6	AA859652	Sense	5′-AAAGGTGTTTCGACTGCATTCTC-3′
		Antisense	5′-CCCCATGTACCAAGCACTGTT-3′
Prlr	AW142962	Sense	5′-TGTCGCATAAGGTCCCCTCTT-3′
		Antisense	5′-GCTTGGCAATTTGTAGGGAAAG-3′
Pi4KII	BE097981	Sense	5′-CCCCTTTCTCTTTCCTTCTGGTA-3′
		Antisense	5′-ACAGCAAGTTCCAGGACAGTCA-3′
Actn1	BE119221	Sense	5′-AAGAAGGCGGTGTCTGTAAGCT-3′
		Antisense	5′-CCGTCCCTTGGCTTTGAA-3′
Pvrl3	AW525315	Sense	5′-GGCAAGACACTGGTTCTACACAAT-3′
		Antisense	5′-AAGGCCCGAAGAATGTTTTTC-3′
Rai3	BI276110	Sense	5′-GGAGCAAGTGCCAGGAATTTAT-3′
		Antisense	5′-CAGTTTTTTCCAGCCAGGAGAA-3′

Actn1, actinin α1; Chi3l1, chitinase 3-like 1; Pi4KII, phosphatidylinositol 4-kinase type 2α; Prlr, prolactin receptor; Pvrl3, poliovirus receptor-related 3; Rai3, retinoic acid induced 3; Slc2a3, solute carrier family 2 (facilitated glucose transporter) member 3; Slc16a6, solute carrier family 16 (monocarboxylic acid transporters) member 6.

adirect/ab?cmd=catNavigate2&catID=601267) (n = 5/histological preparation). For measurement of transcript levels of chitinase 3-like 1, solute carrier family 2 (facilitated glucose transporter) member 3, solute carrier family 16 (monocarboxylic acid transporters) member 6, prolactin receptor, phosphatidylinositol 4-kinase type 2α, actinin α1, *Pvrl3*, and retinoic acid induced 3, primer sets were designed using Primer Express software (Version 2.0; Applied Biosystems), and the corresponding primer sequences are shown in Table 1. Amplified transcript levels were measured with the SYBR Green detection system (n = 5/histological preparation). For quantification of expression data, a standard curve method was applied using the first-round antisense RNA prepared for microarray analysis from NTF as a standard sample. Expression values were normalized to two housekeeping genes, glyceraldehyde 3-phosphate dehydrogenase and hypoxanthine-guanine phosphoribosyltransferase, as described previously.[14]

Immunohistochemistry. The cranial halves of the bilateral thyroids of SDM-promoted animals were subjected to fixation in 10% phosphate-buffered formalin (pH 7.4) solution for 2 days at room temperature, and prepared for histopathological examination. In untreated controls and DHPN-alone cases, whole thyroid tissue was fixed in buffered formalin and prepared similarly.

Immunohistochemistry was carried out with antibodies against ceruloplasmin (clone 8, mouse IgG_1, 1:50; BD Transduction Laboratories, San Jose, CA, USA), Ccnb1 (clone V152, mouse IgG_1, 1:100; Thermo Fisher Scientific Inc., Fremont, CA, USA), Cdc2 (clone A17, mouse IgG_{2a}, 1:200; GeneTex, San Antonio, TX, USA), thyroglobulin (clone SPM221, mouse IgG_1, 1:250; Spring Bioscience, Fremont, CA, USA), Pvrl3 (goat IgG, 1:100; R&D Systems, Minneapolis, MN, USA), and Id3 (rabbit IgG, 1:100; ProteinTech Group, Chicago, IL, USA). For confirmation of positive immunoreactivity of antigens examined, normal rat tissues, such as the liver for ceruloplasmin,[19] duodenal mucosa for Ccnb1 and Cdc2, and thyroid for thyroglobulin,[20] Pvrl3, and Id3, were used. For each antigen, subcellular or extracellular localization was examined and compared to the cases previously reported.[21–26] Optimal conditions for antigen retrieval were also determined using positive control tissues. For antigen retrieval, deparaffinized sections were heated in 10 mM citrate buffer (pH 6.0) by autoclaving for 10 min before incubation with the Ccnb1 and Pvrl3 antibodies, or for 20 min before incubation for ceruloplasmin, Cdc2, and Id3. No antigen retrieval treatment was carried out for thyroglobulin. Immunodetection was carried out utilizing a Vectastain Elite ABC kit (Vector Laboratories, Burlingame, CA, USA), with 3,3′-diaminobenzidine/H_2O_2 as the chromogen, as described previously.[15] As negative controls for immunoreactivity, normal serum from mouse, goat, or rabbit was applied to rat positive control tissues with appropriate dilutions instead of the primary antibodies. Sections were counterstained with hematoxylin.

Analysis of immunoreactivity. For all antigens examined in the present study, immunoreactivity was essentially unaltered in the thyroids between the groups of untreated controls and DHPN alone, and these animals did not develop any proliferative lesion. Therefore, immunoreactivity scores in these groups were counted together and represented as 'normal follicular cells' with three randomly selected microscopic areas at 200-fold magnification in one animal. Animals examined for 'normal follicular cells' were nine untreated controls and five treated with DHPN. In the SDM-promoted cases, immunoreactivity scores were counted in the histological categories of NTF, FFCH + Ad, and Ca. With regard to NTF, three randomly selected microscopic areas at 200-fold magnification were subjected to evaluation for each animal. With Ca, both capsular invasive and parenchymal Ca were analyzed. Immunoreactivity in each histological type was not essentially different between the cases after 10 and 15 weeks of promotion, and therefore immunolocalization scores were counted together for these two time points. The numbers of animals examined for proliferative lesions and surrounding NTF were 10 and 11 after 10 and 15 weeks of promotion, respectively.

For ceruloplasmin, Ccnb1, Cdc2, Id3, and thyroglobulin, immunolocalization was scored as 0 (negative), 1 (slight), 2 (moderate), or 3 (prominent). In the case of Pvrl3, scores were 0 (negative), 1 (partially positive), or 2 (positive). Detailed criteria for the immunoreactivity for each molecule given in Table 2 were determined after due consultation of two independent pathologists. Immunoreactivity score in each lesion was double-checked by one pathologist and then cross-checked by another pathologist.

Data analysis. Expression values from the real-time RT-PCR were analyzed by Student's or Welch's t-test following a test for equal variance. Scores for immunoreactivity were assessed with Mann–Whitney's U-test, comparing NTF and normal follicles, FFCH + Ad or Ca. For the microarray data, the statistical analysis was carried out with GeneSpring software, and the significance

Table 2. Scoring criteria for immunohistochemical localization

Molecule	Immunolocalization for evaluation	Score of immunoreactivity			
		0	1	2	3
Ceruloplasmin	Luminal cellular surface	—	Weakly positive, a few follicles	Strongly positive, focal follicular populations	Strongly positive, majority of follicles
Ccnb1	Cytoplasm	—	Weakly positive, a few cells	Weakly positive, majority of cells	Strongly positive, majority of cells
Cdc2	Cytoplasm and nucleus	—	1–10 cells/400× field	10–30 cells/400x field	> 30 cells/400× field
Thyroglobulin	Cytoplasm	—	< 20% cells	20–70% cells	> 70% cells
Pvrl3	Intercellular membrane	—	Focally positive	Entirely positive	Not applied
Id3	Nucleus	—	Weakly positive, a few cells	Weakly positive, majority of cells	Strongly positive, majority of cells

Ccnb1, Cyclin B1; Cdc2, cell division cycle 2; Id3, inhibitor of DNA binding 3; Pvrl3, poliovirus receptor-related 3.

of gene expression changes was analyzed by Student's *t*-test or ANOVA between NTF and normal follicles, FFCH + Ad or Ca.

Results

Microarray analysis. As genes showing altered expression specifically in FFCH + Ad, 40 examples were upregulated and 20 examples were downregulated, as compared with surrounding NTF (Table 3; Supporting Tables S1, S2). In the Ca cases, the numbers of genes specifically upregulated and downregulated were 69 and 142, respectively. Representative genes with known annotations associated with carcinogenesis are listed in Table 3. Interestingly, a cluster of cell cycle-related genes were found to be upregulated specifically in FFCH + Ad, such as ubiquitin-like with PHD and RING finger domains 1, kinesin family member 23, cyclin A2, M-phase phosphoprotein, topoisomerase (DNA) 2α, Cdc2 homolog A, Ccnb1, and cyclin-dependent kinase inhibitor 3. Extracellular matrix proteins, laminin γ2, and fibronectin 1 also showed upregulation in FFCH + Ad. No particular functional cluster was observed for downregulated genes in FFCH + Ad cases. Among the upregulated genes in Ca, examples with functions in transport (ceruloplasmin) and biosynthesis (thyroglobulin) were found, whereas downregulated genes typically involved functions in tumor suppression, such as: decorin, reversion-inducing-cysteine-rich protein with kazal motifs, creatine kinase mitochondrial 1 ubiquitous, retinoblastoma 1, lysyl oxidase, and NAD(P)H dehydrogenase quinine 1. Transcript levels for genes encoding signal transduction molecules and transcription factors were also downregulated in Ca. All isoforms of Id were found to be reduced.

With regard to genes showing altered expression in common in FFCH + Ad and Ca, totals of 93 and 53 were upregulated and downregulated, respectively (Table 4; Supporting Table S3). Upregulated genes included examples linked to transport, cell proliferation, and tumor progression. In particular, multiple gene probes in the array showed increased signals for ceruloplasmin and solute carrier family 16 (monocarboxylic acid transporters) member 6. Among the genes that showed downregulation, no particular functional clusters were apparent. Two gene probes for *Pvrl3* in the array demonstrated downregulation. Real-time RT-PCR for validation of microarray data was carried out for 11 genes showing commonly altered expression with FFCH + Ad and Ca, eight upregulated and three downregulated, the results being summarized in Table 5. In both FFCH + Ad and Ca, many expression changes were similar with the two analysis systems, despite a lower magnitude of alteration observed with PCR data for the upregulated genes when the values were normalized to hypoxanthine-guanine phosphoribosyltransferase levels. With regard to downregulated genes, variability of PCR data in the NTF after normalization to the hypoxanthine-guanine phosphoribosyltransferase level was slightly higher than with glyceraldehyde 3-phosphate dehydrogenase (data not shown), and therefore statistical significance was not attained for FFCH + Ad.

Immunolocalization in the thyroid in relation to proliferative lesions. Ceruloplasmin was immunolocalized mainly at the luminal surfaces of cell membranes of follicular cells, almost specific to the proliferative lesions (Fig. 2a). Diffuse or granular immunoreactivity was also observed in the follicular lumina of lesions showing cell surface immunoreactivity. In parallel with the upregulation of transcript levels both in microarray and real-time RT-PCR analyses, immunolocalization of ceruloplasmin was specifically observed in all types of proliferative lesions, with statistical significance in the scores as compared with NTF. Although the intensity was weak, increased cytoplasmic staining was also observed in some Ca.

Ccnb1 was immunolocalized in the cytoplasm of follicular cells with fine granular immunoreactivity (Fig. 2b). In the normal follicles and NTF, weak and sparse immunolocalization was typical. In the proliferative lesions, the expression pattern of this molecule was either sparse or diffuse, and staining was weak with the former and either weak or strong with the latter. In parallel with upregulation of transcript levels in microarray analysis, a significant increase in the immunolocalization scores was observed in FFCH + Ad as compared with surrounding NTF. Although statistically significant elevation was still evident, immunoreactivity was less intense in Ca than in FFCH + Ad.

Immunoreactivity of Cdc2 was strong and localized both to the cytoplasm and nucleus of tumor follicular cells (Fig. 2c). In the normal follicles and NTF, immunoreactive cells were rather few. Although microarray data showed upregulation only in FFCH + Ad, both FFCH + Ad and Ca showed statistically significant increases in the immunolocalization scores as compared with NTF. Ca demonstrated the highest scores.

Thyroglobulin showed strong and granular immunolocalization in the cytoplasm of normal and non-tumor follicular cells as well as diffuse immunoreactivity in the follicular lumina (Fig. 2d). Although microarray data showed upregulation of the transcript levels in Ca, follicular proliferative lesions showed large variability in the immunoreactivity, and Ca showed a significant decrease in immunolocalization scores as compared with NTF.

Pvrl3 showed intercellular membrane immunolocalization in the normal and non-tumor follicular cells (Fig. 2e). With both FFCH + Ad and Ca, in parallel with the downregulation of the transcript levels common to microarray and real-time RT-PCR analyses, statistically significant decreased immunolocalization scores were observed as compared with NTF. However, the magnitude of the decrease in FFCH + Ad was stronger than in the Ca case, contrasting with the transcript data.

Inhibitor of DNA binding 3 showed nuclear immunoexpression in normal and non-tumor follicular cells (Fig. 2f). Although microarray analysis showed statistically significant downregulation of transcript levels only in Ca, statistically significant decreases

doi: 10.1111/j.1349-7006.2009.01094.x

Table 3. List of representative genes with known functional annotations associated with carcinogenesis showing altered expression specifically in thyroid proliferative lesions of each category induced in rats using a two-stage thyroid carcinogenesis model (≥2-fold, ≤0.5-fold)[†]

Gene function	Accession no.	Gene title	Symbol	FFCH + Ad	Ca
FFCH + Ad					
Upregulated genes (of 40 genes in total)					
Cell cycle	BE098732	Ubiquitin-like, containing PHD and RING finger domains, 1	Uhrf1	2.43	1.81
Cell cycle	BE113443	Kinesin family member 23[‡]	Kif23	2.20	1.09
Cell cycle	AA998516	Cyclin A2	Ccna2	2.13	1.29
Cell cycle	BM385445	Topoisomerase (DNA) 2α	Top2a	2.12	1.37
Cell cycle	BE110723	M-phase phosphoprotein 1[‡]	Mphosph1	2.09	1.35
Cell cycle	NM_019296	Cell division cycle 2 homolog A (*S. pombe*)	Cdc2a	2.04	1.45
Cell cycle	X64589	Cyclin B1	Ccnb1	2.01	1.40
Cell cycle	BE113362	Cyclin-dependent kinase inhibitor 3[‡]	Cdkn3	1.97	1.18
Metastasis	BM385282	Laminin, γ2	Lamc2	2.90	1.25
Metastasis	AA893484	Fibronectin 1	Fn1	2.16	1.40
Downregulated genes (of 20 genes in total)					
Metastasis	BE117767	Immunoglobulin superfamily, member 4A[‡]	Igsf4a	0.46	0.73
Cell differentiation	BG666709	N-myc downstream regulated 4	Ndr4	0.50	0.51
Ca					
Upregulated genes (of 69 genes in total)					
Biosynthesis	AI500952	Thyroglobulin	Tg	1.72	2.65
Transport	AF202115	Ceruloplasmin	Cp	1.99	2.45
Transport	BE106526	Solute carrier family 6 (neurotransmitter transporter, GABA), member 11	Slc6a11	1.44	1.98
Cell growth	M57668	Prolactin receptor	Prlr	1.78	2.42
Cell cycle	NM_133578	Dual specificity phosphatase 5	Dusp5	1.74	2.02
Proto-oncogene	NM_012874	v-ros UR2 sarcoma virus oncogene homolog 1 (avian)	Ros1	1.59	1.98
Metastatic regulator	AI175048	Sine oculis homeobox homolog 1 (*Drosophila*)	Six1	1.62	1.96
Glycolysis	BI294137	Hexokinase 2	Hk2	1.20	1.87
Downregulated genes (of 142 genes in total)					
Tumor suppressor	BM390253	Decorin	Dcn	0.76	0.27
Tumor suppressor	AW523759	Reversion-inducing-cysteine-rich protein with kazal motifs[‡]	Reck	0.65	0.32
Tumor suppressor	BI301453	Creatine kinase, mitochondrial 1, ubiquitous	Ckmt1	0.49	0.35
Tumor suppressor	AI178012	Retinoblastoma 1	Rb1	0.75	0.38
Tumor suppressor	NM_017061 (BI304009)	Lysyl oxidase	Lox	0.81 (0.91)	0.39 (0.49)
Tumor suppressor	J02679	NAD(P)H dehydrogenase, quinone 1	Nqo1	0.57	0.42
Signal transduction	U78517	cAMP-regulated guanine nucleotide exchange factor II	Rapgef4	0.65	0.32
Signal transduction	AA945708	Calcitonin receptor-like	Calcrl	0.59	0.34
Signal transduction	BI295477	G protein-coupled receptor 116	Gpr116	0.61	0.45
Signal transduction	NM_030829	G protein-coupled receptor kinase 5	Grk5	0.66	0.48
Cell adhesion	NM_031050	Lumican	Lum	0.99	0.33
Transcription	AF000942	Inhibitor of DNA binding 3, dominant negative helix-loop-helix protein	Id3	0.57	0.33
Transcription	BE116009	Inhibitor of DNA binding 4	Idb4	0.56	0.40
Transcription	NM_053713	Kruppel-like factor 4 (gut)	Klf4	0.67	0.40
Transcription	M86708	Inhibitor of DNA binding 1, helix-loop-helix protein (splice variation)	Id1	0.64	0.44
Transcription	AI008792	Inhibitor of DNA binding 2, dominant negative helix-loop-helix protein	Id2	0.68	0.48
Metastasis suppressor	AI578087 (AW435343)	transmembrane 4 superfamily member 1[‡]	Tm4sf1	0.64 (0.74)	0.36 (0.48)
Apoptosis	AA892770	Glutamate-cysteine ligase, catalytic subunit	Gclc	0.61	0.41
Tumor metastasis	NM_133526	Transmembrane 4 superfamily member 3	Tm4sf3	0.70	0.41

Ad, adenoma; Ca, carcinoma; FFCH, focal follicular cell hyperplasias.
[†]Proliferative lesions were divided into two categories, i.e. FFCH + Ad and Ca.
[‡]Predicted gene identity.

in the nuclear immunolocalization scores were also observed in FFCH + Ad.

Discussion

With the present microdissected lesion-specific gene expression profiling, alteration was found for 60 genes specifically in FFCH + Ad, 211 genes specifically in Ca, and 146 genes in common in both, as compared with surrounding NTF. On selection of these with known annotations associated with carcinogenesis, we found upregulation of cell cycle-related genes specifically in the early proliferative lesions, represented by FFCH and Ad. In the advanced Ca lesions, downregulation of genes related to tumor suppression and those encoding

Table 4. List of representative genes with known functional annotations associated with carcinogenesis showing altered expression in common with all types of thyroid proliferative lesions induced in rats using a two-stage thyroid carcinogenesis model (≥2-fold, ≤0.5-fold)†

Gene function	Accession no.	Gene title	Symbol	FFCH + Ad	Ca
Upregulated genes (of 93 genes in total)					
Adhesion	AA945643	Chitinase 3-like 1	Chi3l1	7.46	8.55
Adhesion	AI169104	Platelet factor 4	Pf4	2.52	3.71
Angiogenesis	NM_021751	Prominin 1	Prom1	4.26	5.53
Transport	NM_012532	Ceruloplasmin	Cp	3.32	4.12
	(AF202115)			(2.43)	(2.79)
Transport	AA901341	Solute carrier family 2 (facilitated glucose transporter), member 3	Slc2a3	2.68	2.53
Transport	AA859652	Solute carrier family 16 (monocarboxylic acid transporters), member 6	Slc16a6	2.28	2.33
	(BG372184)			(2.25)	(2.24)
Cell proliferation	AF411318	Metallothionein	Mt1a	2.11	3.77
Cell proliferation	AA819913	Carbohydrate (keratan sulfate Gal-6) sulfotransferase 1‡	Chst1	2.77	3.75
Cell proliferation	NM_022278	Glutaredoxin 1 (thioltransferase)	Glrx1	3.63	3.70
Cell proliferation	NM_013122	Insulin-like growth factor binding protein 2	Igfbp2	2.51	2.78
Cell proliferation	AI101583	Transient receptor potential cation channel, subfamily V, member 6	Trpv6	2.01	2.25
Cell proliferation	BI290527	T-box 2‡	Tbx2	2.66	2.19
Biosynthesis	BE097981	Phosphatidylinositol 4-kinase type 2α	Pi4KII	2.66	3.36
Signal transduction	NM_012707	Glucagon	Gcg	3.07	2.79
Cell growth	AW142962	Prolactin receptor	Prlr	2.22	2.46
Tumor progression	BE102969	Ets variant gene 4 (E1A enhancer binding protein, E1AF)‡	Etv4	2.62	2.25
Tumor progression	BG379319	Transforming growth factor, beta induced	Tgfbi	3.41	2.41
Tumor progression	BE120425	Calcium/calmodulin-dependent protein kinase II gamma	Camk2g	2.17	1.90
Cell cycle	NM_133309	Calpain 8	Capn8	2.06	2.55
Cytoskeleton	BE119221	Actinin, α1	Actn1	2.11	2.09
Downregulated genes (of 53 genes in total)					
Adhesion	AW525315	Poliovirus receptor-related 3‡	Pvrl3	0.46	0.28
	(AI103913)			(0.44)	(0.31)
Transcription	NM_013060	Inhibitor of DNA binding 2, dominant negative helix-loop-helix protein	Id2	0.47	0.28
Biosynthesis	NM_022276	Glucosaminyl (*N*-acetyl) transferase 1, core 2	Gcnt1	0.44	0.30
Signal transduction	BI276110	Retinoic acid induced 3‡	Rai3	0.48	0.33
Apoptosis	AI227742	Bcl-2-related ovarian killer protein	Bok	0.44	0.36

Ad, adenomas; Ca, carcinomas; FFCH, focal follicular cell hyperplasias.
†Proliferative lesions were divided into two categories, i.e. FFCH + Ad and Ca.
‡Predicted gene identity.

Table 5. Validation of microarray data by real-time reverse transcription-polymerase chain reaction (PCR)

Gene	FFCH + Ad			Ca		
	Microarray	Real-time PCR normalized by		Microarray	Real-time PCR normalized by	
		Hprt	Gapdh		Hprt	Gapdh
Chi3l1	7.40 ± 1.06*	7.35 ± 2.85***	10.73 ± 4.13	8.67 ± 2.67*	8.14 ± 3.49***	14.09 ± 4.61***
Cp	3.29 ± 0.27**	3.18 ± 0.89****	4.69 ± 1.19****	4.12 ± 0.62**	3.50 ± 0.84****	6.15 ± 0.83****
Slc2a3	2.66 ± 0.25**	2.47 ± 0.66****	3.55 ± 0.93	2.52 ± 0.31**	2.41 ± 0.41****	4.15 ± 0.28***
Scl16a6	2.29 ± 0.53**	2.20 ± 0.73***	3.26 ± 1.12****	2.23 ± 0.26**	2.19 ± 0.63***	3.88 ± 0.89****
Gcg	3.07 ± 0.60*	2.37 ± 0.72***	3.46 ± 0.88	2.96 ± 1.21*	2.55 ± 1.17***	4.40 ± 1.69***
Prlr	2.22 ± 0.61*	1.53 ± 0.36	2.21 ± 0.51****	2.51 ± 0.80**	1.87 ± 0.36***	3.23 ± 0.43****
Pi4KII	2.67 ± 0.89*	2.01 ± 0.74	2.96 ± 1.12****	3.30 ± 0.95**	2.17 ± 0.59***	3.84 ± 0.83****
Actn1	2.13 ± 0.47*	1.61 ± 0.48	2.35 ± 0.73****	2.17 ± 0.82*	1.52 ± 0.38	2.67 ± 0.56****
Pvrl3	0.44 ± 0.07*	0.40 ± 0.08	0.59 ± 0.10****	0.31 ± 0.05*	0.35 ± 0.05***	0.62 ± 0.12****
Rai3	0.48 ± 0.06*	0.42 ± 0.06	0.63 ± 0.09****	0.34 ± 0.08*	0.32 ± 0.06***	0.58 ± 0.17****
Gcnt1	0.44 ± 0.08*	0.63 ± 0.14	0.95 ± 0.17	0.31 ± 0.09*	0.37 ± 0.05***	0.67 ± 0.08****

Gapdh, glyceraldehyde 3-phosphate dehydrogenase; Hprt, hypoxanthine-guanine phosphoribosyltransferase.
Values are mean ± SD ($n = 5$) when the expression level in non-tumor follicles was calculated as 1. A single RNA sample for measurement was an equal mixture of total RNA from the same category tissue preparations from two animals.
*,**: Significantly different from non-tumor follicles at $P < 0.05$ and $P < 0.01$, respectively (Student's *t*-test calculated by GeneSpring).
,*: Significantly different from non-tumor follicles at $P < 0.05$ and $P < 0.01$, respectively (Student's *t*-test).

transcriptional inhibitors of Id family proteins appeared specific. These genes may play stage-dependent roles during carcinogenesis. In particular, selective activation of cell-cycle molecules in the early stages is considered to be essential for lesions to undergo efficient replication in response to TSH-stimulation, and loss of tumor-suppressor functions may be necessary for acquisition of a malignant phenotype during the progression stage. As genes upregulated in common in all types of proliferative lesions, we

doi: 10.1111/j.1349-7006.2009.01094.x

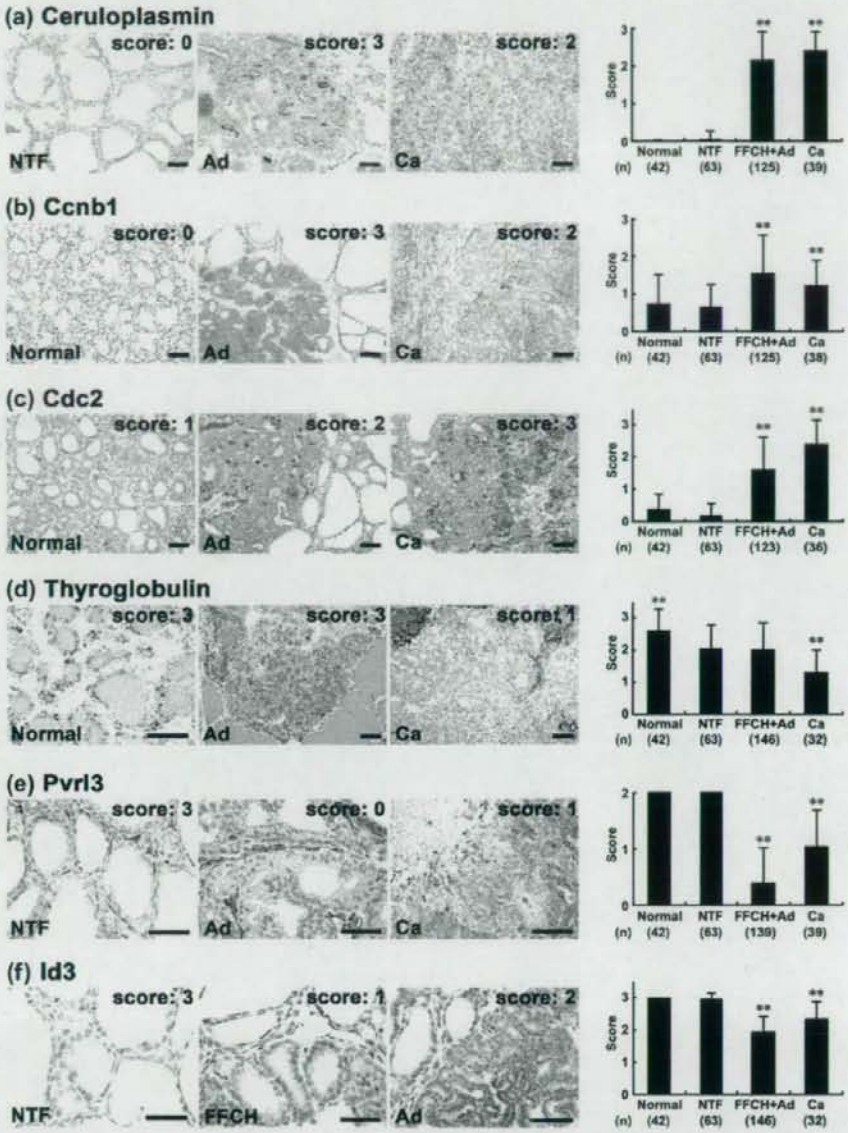

Fig. 2. Immunohistochemical distributions of ceruloplasmin, cyclin B1 (Ccnb1), cell division cycle 2 (Cdc2), thyroglobulin, poliovirus receptor-related 3 (Pvrl3), and inhibitor of DNA binding 3 (Id3) in normal follicular cells of untreated or *N*-bis(2-hydroxypropyl)nitrosamine (DHPN)-treated animals and in proliferative lesions (focal follicular cell hyperplasia [FFCH], adenoma [Ad], carcinoma [Ca]) or surrounding non-tumor follicles (NTF) after promotion with sulfadimethoxine (SDM) for 10 or 15 weeks. (a) Ceruloplasmin in the NTF, Ad, and Ca. Left: NTF nearly lacking ceruloplasmin expression. Middle and right: Ad and Ca showing ceruloplasmin immunoreactivity in the luminal surfaces of cellular membranes of follicular cells. Diffuse or granular immunoreactivity is also evident in the follicular lumina. (b) Ccnb1 in normal follicles, Ad, and Ca. Note fine granular immunoreactivity of Ccnb1 in the cytoplasm of follicular cells. Left: Weak and sparse Ccnb1 localization in normal follicular cells. Middle: Strong and diffuse immunoreactivity in an Ad. Right: Ca demonstrating Ccnb1 immunoreactivity with variable intensity. (c) Cdc2 in normal follicles, Ad, and Ca. Strong Cdc2 immunoreactivity both in the cytoplasm and nucleus of follicular cells. Left: Rather few immunoreactive cells in normal follicles. Middle: An Ad showing sparse Cdc2 immunoreactivity. Right: Note increased numbers of immunoreactive cells in a Ca. (d) Thyroglobulin in normal follicles, Ad, and Ca. Left: Strong and granular thyroglobulin immunoreactivity in the cytoplasm of normal follicular cells as well as diffuse immunoreactivity in the follicular lumina. Middle: Ad showing strong and diffuse thyroglobulin immunoreactivity. Right: A Ca lacking thyroglobulin immunoreactivity in the neoplastic cells. (e) Pvrl3 in the NTF, Ad, and Ca. Left: Diffuse intercellular membrane localization of Pvrl3 in cells comprising NTF. Middle: Ad entirely lacking Pvrl3 expression. Right: Ca showing an irregular and weak intercellular expression pattern. (f) Id3 in NTF, FFCH, and Ad. Left: Diffuse nuclear immunoexpression of Id3 in NTF. Middle: FFCH showing sparse nuclear Id3 expression. Right: Ad showing immunoreactivity in moderate numbers of neoplastic cells. The graphs show scores (mean + SD) for immunohistochemical findings. $^{**}P < 0.01$ versus NTF (Mann–Whitney's *U*-test). (a–f) Scale bar = 50 μm.

also found examples related to cell proliferation, suggesting roles for these molecules consistently throughout carcinogenic processes.

Ceruloplasmin, a copper-containing plasma protein mainly synthesized in the liver, is known to act as a ferroxidase preventing production of toxic Fe and controlling membrane lipid oxidation, while also functioning in angiogenesis and blood coagulation.[19] High levels of antioxidant production likely result from high amounts of reactive oxygen species, which have been implicated in mitogenic signaling and angiogenesis.[27,28] As with high ceruloplasmin levels in the sera of cancer patients, overexpression of ceruloplasmin has been reported in many human malignancies, such as those in the lungs, kidneys, and ovaries.[29–31] With regard to ceruloplasmin in thyroid tumors, it has been demonstrated in follicular cell carcinomas as well as papillary carcinomas, but follicular Ad lack expression.[32–34] In the present study, ceruloplasmin could be immunohistochemically demonstrated in all types of proliferative lesion, in line with transcriptional upregulation. In contrast to the generally benign nature of human Ad, FFCH and Ad in SDM-promoted cases show high cell-proliferation activity similarly to Ca,[9] and this biological behavior may be linked to the increased ceruloplasmin immunoreactivity found in our early proliferative lesions. As discussed by Kondi-Pafiti *et al.*, strong cytoplasmic localization of ceruloplasmin is mainly observed in Ca of human cases, and immunolocalization in luminal secretions (as present in our rat cases) is rare, suggesting a defective catabolism of ceruloplasmin in human Ca.[34]

Cdc2 exerts protein kinase activity by forming complexes with cyclin A2, Ccnb1, and p13suc1 and acts as an active subunit of the M-phase-promoting factor and the M-phase-specific histone H1 kinase.[35] In the present study, increased expression of Ccnb1 and Cdc2, as with other cyclin-related molecules such as cyclin A2, was detected specifically in early proliferative lesions by microarray analysis. Immunohistochemically, we also observed increased expression of Ccnb1 and Cdc2 in both FFCH + Ad and Ca. Chen *et al.* reported coordinated and increased expression of Cdc2 and Ccnb1 in parallel with the pathological grade of human gliomas.[36] They also showed that increased expression of Cdc2 and Ccnb1 contributes to chromosomal instability in tumor cells through alteration of the spindle checkpoint. Thus, the coordinated upregulation of Cdc2 and Ccnb1 observed in the present study might be important as a driving force for both promotion and progression. In another thyroid carcinogenesis study we recently carried out using propylthiouracil as a promoter, a concordant increase of Cdc2 and a cell proliferation marker Ki-67 was found in the proliferative lesions (K. Ago and M. Shibutani, 2008, unpublished data).

Thyroglobulin, a scaffold protein for thyroid hormonogenesis and a storage element for thyroid hormones and iodide, is specifically expressed in the thyroid in response to TSH stimulation.[20] In human malignancies, the presence of thyroglobulin in cancer cells indicates a thyroidal origin.[20] In the present study, although the reason remains unclear, some discrepancy was evident between the mRNA and immunolocalization levels in Ca, the increase in expression on microarray analysis contrasting with the decrease in protein finding. In human thyroid Ca, an inverse relationship between loss of differentiation and thyroglobulin immunoreactivity has been observed, positive cases being less anaplastic,[37] suggesting that the decrease in thyroglobulin in our Ca might have been linked with dedifferentiation, leading to loss of TSH control with malignancy.

Cell adhesion molecules contribute cell-to-cell or cell-to-substratum interactions by homophilic or heterophilic processes.[38] Pvrl molecules, also known as nectins, are adhesion receptors belonging to the IGSF that are involved in cell-to-cell spreading of viruses.[39] Although Pvrl3 protein has not been extensively investigated, it may be a new adhesion molecule expressed on lymphatic endothelial cells.[40] Recent studies have revealed that nectins and nectin-like molecules, in cooperation with integrin and the platelet-derived growth factor receptor, are crucial for mechanisms underlying contact inhibition of cell movement and proliferation.[41] Reduced Pvrl3 expression in all types of proliferative lesions in the present study may reflect acquisition of growth advantage. Interestingly, Pvrl has been shown to be the heterophilic binding partner of another IGSF-type adhesion molecule, tumor suppressor in lung cancer 1 (TSLC1)/IGSF4, a recently identified tumor-suppressor gene.[42,43]

Inhibitor of DNA binding proteins, composed of four members of the helix-loop-helix transcription factors, are known to act as dominant-negative regulators of basic helix-loop-helix transcription factors, and function to inhibit differentiation and enhance cell proliferation.[44,45] In many human malignancies, upregulation of Id has been reported.[46] However, in the present study, all Id isoforms showed downregulation in Ca by microarray analysis, and immunohistochemically, Id3-immunoreactive cells were reduced in all types of proliferative lesions. Similar findings have been reported for human ovarian tumors, in which downregulation of Id3 was noted in 70% of 38 cases.[47] Also, the expression of Id1, Id3, and Id4 was downregulated in microdissected human thyroid Ca compared with surrounding tissues by microarray analysis in one recent study.[48] Although the reason for the inconsistency in the expression alterations between tumor types is not clear, it is possible that gene control mechanisms of Id proteins may differ with the cell type of origin.

In conclusion, we here found differentially regulated genes that may play key roles in early and late stages of thyroid carcinogenesis by microarray analysis of microdissected proliferative lesions developing after promotion with SDM in a two-stage model. Immunohistochemical analysis of representative proliferative lesions indicated facilitation of the cell cycle in early lesions by forming an M-phase promoting factor, as evidenced by the synchronized localization of Ccnb1 and Cdc2, and generation of oxidative stress responses by ceruloplasmin accumulation, as well as reduction of cellular adhesion involving Pvrl3 and cellular differentiation related to transcriptional control by Id3. Decreased expression of thyroglobulin in Ca may reflect dedifferentiation. Although further studies should address particular roles in the processes of thyroid carcinogenesis, the molecules identified in the present study provide pointers to understanding the mechanism of non-genotoxic carcinogenesis and should help in efforts to secure human health.

Acknowledgments

We thank Miss Tomomi Morikawa and Ayako Kaneko for their technical assistance in conducting the animal study. This work was supported by Health and Labour Sciences Research Grants (Research on Food Safety) from the Ministry of Health, Labour, and Welfare of Japan. We all authors disclose here that there are no conflicts of interest that could inappropriately influence the outcome of the present study.

References

1 Thyroid Carcinoma Task Force. AACE/AAES medical/surgical guidelines for clinical practice: management of thyroid carcinoma. American Association of Clinical Endocrinologists. American College of Endocrinology. *Endocr Pract* 2001; **7**: 202–20.

2 Schneider AB, Sarne DH. Long-term risks for thyroid cancer and other neoplasms after exposure to radiation. *Nat Clin Pract Endocrinol Metab* 2005; **1**: 82–91.

3 Kitahori Y, Hiasa Y, Konishi N, Enoki N, Shimoyama T, Miyashiro A. Effect of propylthiouracil on the thyroid tumorigenesis induced by *N*-bis (2-hydroxypropyl) nitrosamine in rats. *Carcinogenesis* 1984; **5**: 657–60.

doi: 10.1111/j.1349-7006.2009.01094.x